TECHNICAL MEMORANDUM

225

Simulation of fog with the ECMWF prognostic cloud scheme

J. Teixeira

Research Department

November 1997

European Centre for Medium-Range Weather Forecasts
Europäisches Zentrum für mittelfristige Wettervorhersage
Centre européen pour les prévisions météorologiques à moyen

SIMULATION OF FOG WITH THE ECMWF PROGNOSTIC CLOUD SCHEME

João Teixeira

ECMWF, Reading, UK

ABSTRACT

A prognostic cloud scheme has been operational at ECMWF since 1995. In this paper the performance of the cloud scheme in simulating fog is assessed. A case study is performed with the one-column version of the ECMWF model in order to analyse how the model reproduces the main mechanisms of fog generation and dissipation. A climatology of the model's fog is produced using data from the ECMWF Re-Analysis (ERA) and compared with climatological data. High resolution (T213L31) operational forecasts with the prognostic cloud scheme are compared with synoptic reports of visibility for Europe. In this context the relation between fog and temperature, on the one hand, and fog and wind speed, on the other, is explored in some detail.

The comparison between the simulated and the observed visibility, in the one-column model case study, shows that the evolution of fog is properly simulated. The analysis of the behaviour of the different parametrized physical processes suggests that the subtle balance between the various processes, fundamental for a realistic fog simulation, is achieved. This study also shows that in radiation fog a cooling process like radiation, that only changes T without changing q is rather essential in order to reach saturation. The comparison between the model's fog climatology and the climatological data shows that the model is able to reproduce most of the major fog areas, particularly over the ocean.

The analysis of the results from high resolution fog forecasts for Europe and the comparison with synoptic observations of visibility shows that the model simulates realistically some of the fog over Europe, particularly at 0 UTC and 6 UTC. At 12 UTC the fog in the model is usually underestimated. In general, the number of situations where the visibility is between 2 km and 11 km is underestimated by the model. It is shown that the model is always slightly closer to saturation than the observations and this might be helping the model in producing fog. The model reproduces the observed behaviour of fog as a function of temperature and wind speed rather realistically.

1. Introduction

Fog is a common meteorological phenomenon and fog forecasting is an important and challenging task. The WMO (1966) defines fog as a suspension of very small water droplets (sometimes ice crystals) in the atmosphere, reducing the horizontal visibility at the Earth's surface to less than 1 km (if the visibility is above 1 km it is called mist). According to Cotton and Anthes (1989) fog typically has a lifetime of 2 to 6 hours and a liquid water content from 0.05 to 0.2 g/kg. Such low liquid water contents are very demanding for any forecasting system.

A simple and instructive way of thinking about the fog generation mechanisms is by representing the thermodynamic state of an air parcel in a Clausius-Clapeyron diagram, where the water vapour pressure (or specific humidity) is plotted against temperature. Taylor's (1917) simple analysis of this diagram, still widely used (e.g. Cotton and Anthes 1989; Stull 1995), shows that fog generation can be conceptually reduced to 3 main processes: cooling (e.g. radiative cooling) by which the temperature is reduced without changing the moisture content; moistening (e.g. evaporation of warm precipitation falling through cooler air) by which the moisture content is increased without changing the temperature; and mixing of air parcels (of which at least one might be unsaturated) that may lead to saturation due to the nonlinearity of the saturation curve given by the Clausius-Clapeyron equation.

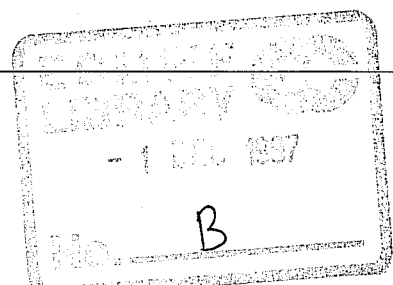

In the real atmosphere all these processes may occur at the same time, although one mechanism might be dominant. Mixing is always present and plays an important role in the formation and dissipation of most fog events. However, without some additional cooling and/or moistening, fog seldom forms by mixing alone. Oliver et al. (1978) conclude that radiation plays a significant role in most surface fogs deeper than a few meters.

In a global NWP model, the most relevant aspect of fog is probably its intimate relation with the existence of low stratus: the lifting of fog from the ground in the morning is typical during radiation fog dissipation and stratus lowering fog is a common event, for example in Coastal California (e.g. Pilie et al. 1979). Fog is also considered to be related to the generation of Arctic stratus (Houze 1993) while the possibility of marine stratus being formed as fog is referred to by Moeng (1993).

The evolution of fog in a NWP model depends on several parametrized physical processes: turbulent mixing, radiation, clouds, condensation and interaction with the surface. A successful forecast of a fog event suggests that a suitable and delicate balance has been achieved between all these different parametrized physical mechanisms.

The first numerical studies of fog used 1D and 2D boundary layer models with a rather simplified physics (e.g. Fisher and Caplan 1963; Zdunkowksi and Barr 1972; Brown and Roach 1976). More recent studies (e.g. Musson-Genon 1987; Turton and Brown 1987) have focused on the interaction with the vegetation (Duynkerke 1991) or on the interaction between radiative transfer and fog microphysics (Bott et al. 1990). Some recent studies used 3D mesoscale models (e.g. Ballard et al. 1991; Golding 1993). A recent introduction to numerical studies of fog can be found in Bergot and Guedalia (1995).

Until quite recently, forecasting fog was made, and still is, by means of empirical rules or statistical methods (see Tremant (1989) for a review). However, in the last few years some numerical models have been developed that are able to forecast fog operationally. The existing models can be divided in the two groups already mentioned: 3D mesoscale models and 1D boundary layer models (sometimes coupled with horizontal advection schemes). A detailed review of operational models for fog forecasting can be found in Reiff (1987).

In some diagnostic cloud schemes used in global NWP models (e.g. Slingo 1987; Campana 1990) no clouds are allowed in the lowest model level (i.e. fog). The main reason is that the existence of fog in the model is detrimental to the forecast due to a positive feedback with the longwave radiative cooling. This is perhaps not surprising because the diagnostic relations were never optimized for fog situations.

Recently a prognostic cloud scheme has been developed at ECMWF, in which cloud-related processes are treated in a more complete and consistent way (Tiedtke 1993). In the first studies of the performance of the new prognostic cloud scheme (Tiedtke 1993; Kvamsto 1993) clouds were still not allowed in the lowest model level. In more recent versions of the scheme clouds are allowed to develop at any model level. So in principle the model is capable of producing fog and it is therefore important at this stage to make an assessment of the capabilities of the new cloud scheme in simulating and forecasting fog and low stratus. Another reason for such work is the fact that studies of fog with global atmospheric (NWP or climate) models are virtually non-existent.

In this paper the first results of such a study are presented. The purpose of this paper is to assess the performance of the prognostic cloud scheme in simulating fog. In section 2, the prognostic cloud scheme is briefly presented and the terms that are of importance in fog situations are described. A detailed analysis of how the model simulates the main mechanisms of fog generation and dissipation in radiation fog is presented in section 3 where the results of a case study with the one-column version of the ECMWF model are shown.

A climatology of the model's fog was produced using data from the ECMWF Re-Analysis (ERA). These results are compared in section 4 with climatological data. In section 5 high resolution (T213L31) operational forecasts with the

prognostic cloud scheme are compared with synoptic reports of visibility for Europe. In this context maps and time series are produced and the relation between fog amount and temperature, on the one hand, and fog amount and wind speed, on the other, is explored in some detail. Finally, in section 6, some conclusions are presented.

2. The ECMWF prognostic cloud scheme

Prognostic cloud schemes started to be implemented in global atmospheric models only very recently. Most of them treat cloud fraction by means of diagnostic relations (e.g. Sundqvist 1988; Smith 1990). Tiedtke (1993) presents a scheme with prognostic equations for cloud fraction and liquid/ice water content. This scheme improved the simulation of clouds considerably in the ECMWF model compared to the diagnostic cloud scheme that was used before (Tiedtke 1993; Kvamsto 1993; Jakob 1995; Miller et al. 1995).

The prognostic cloud scheme is described in detail in Tiedkte (1993). It consists of two prognostic equations, one for liquid/ice water l and one for cloud fraction a:

$$\frac{\partial l}{\partial t} = A_l + CV_l + BL_l + C - E - P - ENT$$

$$\frac{\partial a}{\partial t} = A_a + CV_a + BL_a + C_a - D$$

where A_l and A_a represent the advection of liquid/ice water and cloud fraction, CV_l and CV_a represent the sources of liquid/ice water and cloud fraction from the moist convection processes, BL_l and BL_a represent the source terms of liquid/ice water and cloud fraction due to boundary layer turbulence, C is the condensation/sublimation rate, E is the evaporation rate, P is the precipitation rate, ENT is the destruction of liquid/ice water due to cloud top entrainment, C_a is the generation of cloud fraction by stratiform condensation and D is the dissipation of cloud fraction by turbulent erosion.

The prognostic cloud scheme allows the ice and the liquid water to co-exist (mixed phase) based on a simple quadratic temperature dependence between 0°C and -23°C (see Jakob, 1995).

2.1 The stratiform clouds

In this paper it will be assumed that fog exists in the model when the liquid/ice water content present at the lowest model level (roughly 30m above the surface) is above a certain value. At this level the dominant sources and sinks for the cloud scheme are the stratiform condensation and evaporation terms.

The stratiform cloud part of the scheme is based on the computation of the term $\frac{dq_s}{dt}$ in order to take into account processes like diabatic cooling from radiation. In the case of fog this term is calculated using the temperature tendency due to radiative and turbulent processes.

Condensation and generation of cloud fraction occur when:

$$\frac{dq_s}{dt} < 0$$

In this case the source terms for the cloud fraction and liquid/ice water equation are:

$$C_a = -\frac{1-a}{q_s - q}\frac{dq_s}{dt}$$

$$C = -a\frac{dq_s}{dt}$$

In the stratiform part of the scheme there are two main processes that dissipate the clouds: evaporation due to diabatic heating and horizontal turbulent mixing of cloudy air with environmental air.

Evaporation of liquid/ice water occurs when:

$$\frac{dq_s}{dt} > 0$$

The evaporation term in the liquid/ice water equation is:

$$E = a\frac{dq_s}{dt} + aK(q_s - q)$$

In this equation the two main dissipative processes are present: the first term on the RHS represents the evaporation in an already existing cloud and the second term parametrizes the mixing between cloudy and environmental air (K is a diffusion coefficient that has the value of $10^{-6}s^{-1}$).

Another process that contributes as a sink term for the liquid/ice water is the cloud-top entrainment. The dissipation of liquid water due to entrainment is:

$$ENT = -\frac{1}{\rho}\frac{\partial}{\partial z}(\rho w_e \Delta l)$$

The entrainment velocity w_e is proportional to the change of the longwave radiative flux F_{LW} at cloud top:

$$w_e = \beta\frac{C_p \Delta F_{LW}}{\Delta s_v}$$

with $\beta = 0.5$, S_v being the virtual dry static energy and $\Delta\psi$ represents the jump of the generic property ψ between the cloud top level and the level above.

In the cloud it is assumed that the liquid water is homogeneously distributed. While the liquid/ice water evaporates the cloud fraction remains unchanged dropping to zero only when the liquid/ice water is totally gone. The only sink term for cloud fraction is the one due to mixing between cloudy and non-cloudy air:

$$D = \frac{a}{l_c}K(q_s - q)$$

where l_c is the in-cloud water content.

3. A One-Column model simulation of radiation fog

In order to study in more detail how the ECMWF model handles the physical mechanisms responsible for fog, a fog event that occurred at Cabauw, the Netherlands, 3 August 1977, was simulated. This particular fog situation has already been studied using 1D boundary layer models developed by Grandin (1983) and Musson-Genon (1987) (hereafter referred to as M87) among others. The data used in this study was taken from M87.

The one-column version of the ECMWF model is based on the global NWP model and integrates a set of 6 prognostic equations (u, v, T, q, a and l) for a column of the atmosphere. In the soil there are evolution equations for the temperature and wetness of the different soil layers plus an evolution equation for the skin temperature and the skin water content. The one-column model can be used with prescribed external forcing: the zonal and meridional components of the geostrophic wind, the vertical velocity and the horizontal advection of the atmospheric variables. The surface pressure is kept constant. The vertical advection is computed as part of the one-column integration using a Semi-Lagrangian scheme. The height of the 5 lowest model levels is roughly 30m, 150m, 360m, 640m and 990m.

The following set of physical parametrizations are in the version of the ECMWF Integrated Forecasting System (IFS) used here. The radiation parametrization is based on a band emissivity scheme for the longwave parametrization and a delta Eddington scheme for the shortwave parametrization (Morcrette 1990). The cloud scheme is the one described briefly in section 2 and presented in detail in Tiedkte (1993). The moist convection is parametrized by using a mass-flux scheme and is described in Tiedkte (1989). The vertical diffusion parametrization is based on a K-diffusion approach with a K-profile closure (Beljaars and Betts 1993) for the unstable boundary layer, a Ri-number dependent diffusion coefficient for stable situations above the surface layer (Louis et al. 1982), and a Monin-Obukhov type closure in the surface layer (Beljaars and Holtslag 1991). The soil/surface scheme consists of a skin layer and four soil levels (Viterbo and Beljaars 1995). The sub-grid scale orographic scheme is described in Lott and Miller (1997).

The data used to initialize the one-column model is described in M87, and consists of vertical profiles of the mean variables as initial conditions at 0 UTC, 3 August 1977, and constant values of the geostrophic wind and temperature advection in the layer from 0 to 200m. Advection of heat and moisture are not known very accurately for this situation. M87 has made an estimate for temperature advection of about -0.18 K/day in the layer up to 200m. Moisture advection is assumed to be negligible. In the current one-column simulations the estimates for advection are as in M87.

3.1 A simulation with the standard version of the model

To compare model results (liquid/ice water content) with the observed visibility the following empirical relation between visibility and liquid water is used (Kunkel 1984):

$$VIS = -\frac{\ln(0.02)}{\beta}$$

where VIS is the model derived visibility and $\beta = 144 \cdot 7(\rho l)^{0.88}$, with l being the lowest model level liquid/ice water. This equation will be used throughout the paper and is illustrated in fig. 1.

The time evolution of the simulated visibility at the lowest model level is presented in fig. 2 together with the visibility observations from the Cabauw tower at the 30m level. The model results are reasonable: the onset of fog is only half an hour late, the lowest values of visibility are close to the observations and the dissipation stage is also properly forecasted.

To understand better the time evolution of this fog situation it is shown in fig. 3 the Clausius- Clapeyron diagram for the model's lowest model level, where the values of q and q_s are plotted versus T. The dots and the numbers represent the hours of simulation (in UTC). Three different periods of the fog's evolution can be distinguished in fig. 3: (i) during the first period, from 0 UTC until 4 UTC, the values of T and q are located on a mixing line that represents the way in which level 31 is evolving towards saturation; (ii) when saturation is reached a second stage starts, until 6 UTC, in which the fog

is intensifying, more liquid water is being produced and T and q keep decreasing but remain on the saturation line and (iii) after 6UTC and until roughly 7.30 UTC a third period starts in which the fog is dissipating, the liquid water decreasing and T and q increasing but still on the saturation line.

In order to assess the role of the different parametrized physical processes on the fog's evolution, in fig. 4a it is shown the lowest model level temperature tendencies (in K/day) and in fig. 4b the lowest model level specific humidity tendencies (in g/kg/day), produced by each one of the parametrizations, during the simulation period. Fig. 4a shows the temperature tendencies from the radiation parametrization (both longwave and shortwave), the vertical diffusion parametrization, the cloud parametrization, the total tendency and also the horizontal advection tendency (constant during the simulation and equal to -.18 K/day). Figure 4b shows the corresponding tendencies for the specific humidity.

The three different periods can be clearly distinguished from these figures. From 0 UTC until the onset of fog the cooling tendencies from radiation and vertical mixing are almost constant in time and with similar values, the vertical mixing being a bit higher than the radiation tendency. During this period the total tendency is nearly constant and around -.75 K/day. In terms of specific humidity during this period the vertical diffusion is generating an almost constant negative tendency of around -0.2 g/kg/day.

Around 4 UTC (about half an hour after the onset of fog) the liquid water starts to increase substantially (as can be inferred from fig.2) and reaches values that are radiatively important. At this stage the longwave cooling increases and reaches a stationary peak of around -2.5 K/day between 5 UTC and 7 UTC. The condensation heating produced by the cloud scheme becomes also relevant reaching a peak value of around 1.5 K/day at 5 UTC, decreasing then to negative values between 7 and 7.30 UTC. After the onset of fog the cloud scheme produces negative tendencies of moisture that dominate the total tendency around 5 UTC when they reach a value of around -0.6 g/kg/day.

After sunrise the skin temperature increases very fast and around 5 UTC it becomes higher than the temperature at the lowest model level. As a consequence the vertical diffusion tendency changes sign and increases until it reaches a peak value of around 5 K/day for temperature and 1.5 g/kg/day for moisture at 7 UTC. Mainly due to this effect the total tendency changes sign and begins to warm and moisten the lowest model level just before 6 UTC reaching a peak value of 3 K/day for temperature and 1.6 g/kg/day for moisture around 7.30 UTC which is the time the fog has disappeared.

3.2 A sensitivity study to the impact of the radiative cooling of the lower atmosphere

The notion that the radiative cooling of the surface has a fundamental role on the development of radiation fog is an established idea, at least since Taylor (1917). However, it was only recently shown (Brown and Roach 1976) that for a proper numerical simulation of radiation fog the longwave cooling of the lower atmosphere had to be included in the model.

To study the impact of the longwave atmospheric cooling in radiation fog the same case was simulated but with the atmospheric radiation tendencies set to zero. In this simulation the lowest model level did not get close enough to saturation and as a consequence the model did not produce fog as can be seen in the Clausius-Clapeyron diagram shown in fig. 5. The cooling and the drying associated with the mixing between 0 UTC and 5 UTC is not enough to saturate the lowest model level.

Another sensitivity test performed was to switch off not only the atmospheric radiative cooling but also the horizontal cold air advection. Again, in this case the model did not produce fog. In fig. 6 a Clausius-Clapeyron diagram, of the lowest model level, for the first 5 hours of these 3 different experiments is shown: control, control with no radiative cooling of the atmosphere and control without radiation and horizontal cold advection. What can be seen is that the thermodynamic state of the lowest model layer always evolves along a mixing line during the first hours of the simulation or until the onset of fog. However, these 3 mixing lines are all different and it can be seen that the model needs a cooling process like

radiation, that only changes T without changing q, to make the mixing line deflect towards an horizontal line in order to reach saturation.

The simulation of this radiation fog event by the ECMWF one-column model can be seen as a good example of a combination of the simple cooling and mixing mechanisms referred in the introduction as the primary processes that are responsible for fog generation.

4. Simulated climatology of fog with the prognostic cloud scheme

A climatology of the model's fog was produced using data from the ECMWF Re-Analysis (ERA). The ERA project has produced a new 15 year data set of assimilated data for the period 1979 to 1993. ERA was produced using the ECMWF Integrated Forecasting System (IFS), that contains both the model and the analysis part of the data assimilation system. For more details about ERA see Gibson et al. (1997). The main model features are: it is a global spectral model with T106 resolution, it has an equivalent Gaussian grid of 1.125^{o} resolution, it has 31 vertical levels and the advection scheme is Semi-Lagrangian. For more details about the dynamics see Ritchie et al. (1995). The physical parametrizations are the ones briefly described in section 3.

To produce the fog climatology 5 years of data were analysed, from 1985 to 1989. The daily 6, 12, 18 and 24 hour forecasts were used to calculate the frequency of occurrence of fog in the model. These values are estimated by computing the frequency of occurrence of values of liquid/ice water in the lowest model level, higher than 0.016 $g.kg^{-1}$. This value roughly corresponds to an horizontal visibility of 1 km in the relation between liquid water and visibility proposed by Kunkel (1984). The frequency of occurrence of fog in the model is halved in order to make the model climatology more compatible with the Warren et al. (1986, 1988) climatology. Warren et al. (1988) suggest that the frequency of fog at a distance and fog within the past hours (which is not included in the observational climatology but is part of the model's climatology) is roughly of the same magnitude as the frequency of "sky obscured" due to fog.

The observed frequency of occurrence of "sky obscured" due to fog is taken from the cloud climatology of Warren et al. (1986, 1988). This climatology is based exclusively on surface observations, either ships at sea or land stations. The climatology results represent averages of 30 years (1951-1981) of data for the oceans and 10 years (1971-1981) for the land areas.

4.1 December-January-February

Figure 7 shows the frequency of occurrence of fog in the model, for the December-January- February (DJF) period. Fig. 8 is taken from the cloud climatology of Warren et al. (1986, 1988) and shows the observed frequency of occurrence of "sky obscured" due to fog for the same period. The first contour is at 2% and the contour interval is 5% for both plots.

Comparing both figures, it can be seen that the simulation of fog over the ocean is good. The model reproduces the major fog areas over the Southern ocean. This maximum of fog frequency during the austral summer could be associated with a maximum of stability in the lower troposphere for that time of the year (Klein and Hartmann 1993). The model is also able to reproduce approximately the regions where fog frequency around Antarctica reaches maximum and minimum values. Some fog over the ocean is also produced by the model in observed fog areas like close to the west coast of Greenland, the Bering Strait, the coast of Newfoundland and in some parts of the North-East Pacific.

The model simulates reasonably well some of the main areas of fog in Europe, except for some parts of the Iberian Peninsula where there seems to be a lack of fog. The fog in areas along the North Mediterranean coast and close to the Black and the Caspian sea is well reproduced. Fog in Scandinavia, particularly around the Baltic Sea, is well simulated by the model. Fog in Eastern China is also reasonably well captured by the model.

As it can be seen in fig. 8 winter fogs can be frequent along the coast of the Gulf of Mexico. According to Petterssen (1969), the drainage into the Gulf of cold, fresh water from the rivers, coastal bays and estuaries causes fog to form when there is a warm and moist flow from the south. The model reproduces some of the fog in this region. In the west coast of the United States fog frequency is underestimated by the model.

In mountain areas such as parts of Canada, Northwest United States, Mexico, New-Guinea and particularly around the Andes the model is producing too much fog when compared to climatology. According to Barry (1981), fog is a prominent feature of most mountain areas and depends very much on local orography. Therefore model and observations are difficult to compare in mountainous areas; The model does not have the resolution to represent the details of the topography and the density of observations tends to be low in these areas.

4.2 June-July-August

In fig. 9 the values of frequency of occurrence of fog in the model, for the June-July-August (JJA) period, are presented. Fig. 10 is taken from the cloud climatology of Warren et al. (1986, 1988) and shows the observed frequency of occurrence of "sky obscured" due to fog for the same period. The first contour is at 4% and the contour interval is 10%.

Comparing both figures it can be seen that again over the ocean the model performs well. In fact, the model is able to capture the areas over the ocean where fog is most frequent during the Northern Hemisphere (NH) summer, particularly in the Western parts of the Pacific and the Atlantic ocean. Close to Newfoundland the model is performing very well. However, over the western Pacific the peak values of fog frequency are underestimated by the model.

The fog that occurs during the NH summer all over the Arctic ocean and neighbouring coastal regions is also well simulated, with some of the peak regions like the ocean areas North of Iceland being reasonably well captured. Fog is produced by the model in some areas of the Southern ocean even during the Southern Hemisphere (SH) winter. However, the number of observations in that area, especially during this time of year, is very small, which makes the validation of model results virtually impossible.

As in the DJF season, the model misses some of the fog observed at the west coast of continents, on the margins of the oceanic subtropical highs. The reasons for this problem will be explored in section 4.3.

During the NH summer, the areas over land where fog is most frequently observed are coastal regions (Newfoundland, North-East Asia or the coastal areas of the Arctic ocean) that are associated with ocean areas with a high frequency of fog. As seen before, the model seems to simulate well the fog in these regions.

Close to the east coast of continents in the NH summer, the high fog frequency is associated with large scale advection of warm and moist air, over ocean regions with large gradients of SST. The success of the fog forecast in these areas is mainly related to the ability of the model to simulate realistically the low level flow and the large scale advection of temperature and moisture over these ocean areas.

From fig. 8 and fig. 10 it can be seen that in some areas of the tropical rain forests, particularly in the Congo basin, fog is expected to exist. Radiation fogs, formed at dawn, frequently occur over the tropical forests (e.g. Ratisbona 1976) due to the high moisture content of the air. As in the DJF season, the model is reasonably successful in simulating fog over the tropical forests of Africa.

Finally, the model reproduces the climatological observation that over ocean, more fog occurs in the Summer Hemisphere and, over land, more fog occurs in the Winter Hemisphere.

4.3 Fog near the west coast of continents

There are areas at the west coast of continents, on the margins of the oceanic subtropical highs, where the model does not generate fog as observed. These regions include the west coasts of the United States, South America and South Africa and the coast of Namibia. Since on many occasions the evolution of fog is coupled with the evolution of low stratus clouds, the model performance in simulating stratus is analysed.

The global distribution of low cloud cover produced by ERA for the period of June-July- August of 1985 to 1990 is presented in fig. 11. As for fog the daily 6, 12 18 and 24 hour forecasts were used. In comparing fig. 11 with climatological data for low stratus distribution (Warren et al. 1986, 1988) for the same period JJA (fig. 12), it can be seen that the model with the prognostic cloud scheme produces a realistic distribution of low clouds. A similar conclusion was drawn by Tiedtke (1993): a comparison to ISCCP data for July 1987 shows that the model produces realistic low and middle level clouds. In fig. 12 there are very few contours south of around 40°S because there are not enough observations to develop a statistically significant climatology.

Returning to the problem of why the model misses fog at the west coast of continents and comparing fig. 11 and 12, it can be seen that the model does not generate enough clouds in the stratocumulus areas and they are also shifted to the west.

The relation between fog and stratus at the west coast of continents is reasonably well documented and stratus lowering fog events are common, for example in coastal California (Oliver et al. 1978; Pilie et al. 1979). Taking this into account it is likely that the lack of fog at the west coasts is connected with this lack of stratocumulus and its westward shift.

Apparently the model has difficulties in simulating fog events that are related to stratus since the physical processes that according to Pilie et al. (1979) and Oliver et al. (1978) dominate this stratus lowering fog situations, like drizzle or turbulent mixing directly induced by cloud top radiative cooling, are not very well parametrized by the model.

5. High resolution fog forecasts over Europe

The prognostic cloud scheme was implemented operationally in the ECMWF model in April 1995. This version of the ECMWF model has already been described in the previous sections and the reader is referred to Miller et al. (1995) for a detailed account of the changes introduced operationally with this model version. The operational model has horizontal spectral resolution T213 which corresponds to a Gaussian grid with 60km resolution. To initialize the cloud fields the first guess results are supplied as cloud initial state for the next first guess or forecast (Jakob 1995).

The observational data that is used to validate the quality of the high resolution fog forecasts is composed by the SYNOP observations distributed by the WMO for the period from September 1995 to January 1996. The following observed quantities are used: wind speed at 10m height, temperature and specific humidity at 2 m height and visibility.

The relation between visibility and liquid water content (Kunkel 1984) is used in order to compare the fog forecasts with the observations of visibility. For the fog verification maps the model liquid/ice water content is converted to visibility and compared with the observed visibility. In the case of time series plots or the computation of average values of fog amount, for the model and the observations, it is the observed visibility that is converted to liquid/ice water content and compared with the liquid/ice water content of the model.

5.1 Fog verification maps over Europe

Fog verification plots for Europe are shown for 0 UTC and 12 UTC. In these plots the 60 and 72 hour forecasts of liquid/ ice water content at the lowest model level are shown, together with the visibility reported by the synoptic stations for the same period. Only the values from the stations that report visibility less than 6 km are shown. When the number 0 is shown it means that the station is reporting values between 0 and 1 km of visibility and so on up to number 5. The liquid water

contours are 0.002, 0.007, 0.016 and 0.1 g/kg. These values correspond roughly to values of horizontal visibility of 6 km, 2 km, 1 km and 200 m respectively (Kunkel 1984).

Several of these plots have been analysed for the period from September 1995 to January 1996. Figures 13 and 14 (corresponding to verification at 0 and 12 UTC of 5 October 1995 respectively) are good examples for this period. Some typical features can be recognized. The model produces more fog at 0 UTC than at 12 UTC. This also happens in nature but not to such a degree. Some areas of fog in Central Europe are not well forecasted. Forecasted fog in some areas of the Baltic Sea coast is verified by the observations. Observed fog in the Alpine regions is not well forecasted at 12 UTC but is reasonably forecasted at 0 UTC, although not necessarily at the exact locations.

Figures 15 and 16 (corresponding to verification at 0 and 12 UTC of 13 October 1995 respectively) represent a particularly successful case of fog forecasting. It can be seen that most of the low visibility (less than 1 km) stations in Central Europe at 0 UTC are covered by the liquid water contours. However, at 12 UTC, when the observed visibility in most of Central Europe increases to values of 3/4 km, the liquid water in the model disappears almost completely.

In general, the model reproduces some of the major areas of fog and mist in Europe, however, it tends to underestimate the total amounts. Also, the situations where the model derived visibility is between 2 km and 6 km are extremely rare, whereas in nature this is very common.

In order to see whether this is a model characteristic, the distribution of the number of fog events (observations and forecasts) for different values of liquid/ice water is plotted in fig. 17. This comparison uses the 30, 36, 42 and 48 hour forecasts and the synop observations for Europe for January 1996. The total number of events (including "fog" and "no fog" events) is around 100000. The observed visibility is converted to liquid/ice water content. The number of events is distributed in intervals of 0.001 g/kg of liquid/ice water content, except for the first interval that is from 0 g/kg to 0.0005 g/kg.

Figure 17 shows that the number of events of liquid/ice water content less than 0.0005 g/kg in the model are around 80000 whereas for the observations this number is much smaller: around 20000. The number of events where the liquid/ice water is between 0.001 and 0.006 g/kg (which roughly corresponds to a visibility between 11 km and 2 km) is largely underestimated by the model when compared with the observations. Above 0.007 g/kg the number of events produced by the model compares reasonably well with the observations

Three possible reasons for the model underestimation of fog/mist in the visibility range between 2 km and 11 km are that: (i) other physical factors like rain, drizzle, snow, dust or atmospheric pollutants can limit the horizontal visibility, (ii) the parametrization of fog still misses some generation or dissipation processes and (iii) the empirical relation used to estimate the visibility from the liquid/ice water content was calibrated under very specific circumstances and its range of validity is exceeded.

5.2 Time series for Europe for January 1996

Time series are produced for Europe (defined by the coordinates 35°N, -10°W, 65°N, 50°E) and two European sub-regions where a comparison between 30, 36, 42 and 48 hour forecasts and synop observations is performed for January 1996. The total number of observations is around 100000. The relation between visibility and liquid water content proposed by Kunkel (1984) is used to convert the observed visibility to liquid/ice water content.

In fig. 18 the time series of liquid/ice water content (which will be often referred to as fog) for the synop observations and forecasts (30, 36, 42 and 48 hour) for Europe is plotted. The results shown can be considered good particularly at 0 UTC and 6 UTC when the forecast values are close to the observations. However, in some occasions the forecasted values are higher than the observed ones. During the day (12 UTC) the fog in the model is usually underestimated which confirms the results from section 5.1.

In fig. 19 the equivalent time series for the 2 m temperature is shown. The most striking feature is the almost constant negative temperature bias of around -4°C. In theory these unrealistic cold temperatures could bring the model closer to saturation than in reality, which could then lead to more frequent fog in the model. It should be mentioned that the 2 m temperature cold bias problem is much less serious in recent versions of the model due to changes in the surface and vertical diffusion schemes (Viterbo et al. 1998).

In order to verify if the model is actually closer to saturation than the observations the average state of saturation of the surface layer for the model and the observations was analysed. In order to do that, the forecasted and observed values of the 2m temperature versus the 2m specific humidity were plotted. The same data set as for the time series is used. In fig. 20 the following is shown: the average 2m specific humidity as a function of 2m temperature (for intervals of 1°C) for both the model and observations, the saturation specific humidity (for liquid and ice water) for the standard atmospheric pressure of 101325 Pa and in dots all the model forecasts. Some of the dots look like they are supersaturated because the saturation curve represented in fig. 20 is calculated using the standard pressure and not the atmospheric pressure that corresponds to one particular dot.

What can be seen in fig. 20 is that the observations and the model have a lower relative humidity at higher temperatures than at lower temperatures. The model is always slightly closer to saturation than the observations. This is probably due to the cold bias of the model which does not go along with a similar dry bias. This might enhance the model's fog production.

However, the direct correlation between fog in the model and the temperature bias (not shown) shows that the average forecasted liquid/ice water content does not change significantly with the temperature bias. This is the case for biases that range from -20°C to 10°C and shows that there is no direct correlation between the cold bias and the performance of the fog forecast.

Two particular areas of Europe were also chosen to be analysed: (i) area 1 (50°N,0°E, 55°N, 20°E) that includes coastal areas of the United Kingdom, Belgium, the Netherlands, Germany, Denmark and Poland (ii) and area 2 (45°N, 15°E, 55°N, 35°E) that includes continental areas of Central Europe. In both these areas topography does not play a significant role in the development of fog.

The time evolution of the forecasted and observed fog for area 1 is plotted in fig. 21. It can be seen that, although the forecast of fog is not as consistent as in fig. 18, it is still reasonably good. However, in this area fog is underestimated by the model when compared with the observations. In area 2, as can be seen in fig. 22, the quality of the fog forecasts is also less consistent than in fig. 18. But in this case the general underestimation of fog by the model seen in fig. 21 is not so clear because the model has spells with overestimation of fog as well.

From fig. 23, where the 2 m temperature time series of forecasted and observed values for area 1 is plotted, and comparing it to fig. 21, it can be seen that both the model and the observations seem to produce less fog when the temperatures decrease substantially below 0°C. Comparing the fog in area 1 shown in fig. 21 with fig. 24 where the time evolution of 10m wind speed for the model and the observations is shown, it can be seen that it is during the period between day 16 and 18, when the wind speed reaches its lowest value, that the amount of fog is the highest. From day 17 to day 24 the wind speed increases from 2.5 m/s to 8 m/s and fog decreases considerably, both in the model and in the observations, to an almost negligible value. These two comparisons suggest a physical relation between the amount of observed and forecasted fog and the wind speed and temperature, which will be explored in the next section.

5.3 Fog versus temperature and wind speed

The statistical relation between the amount of fog and parameters like the 2m temperature and the 10m wind speed, both in the model and in the observations, is analysed further by plotting liquid/ice water content versus 10m wind speed and 2m temperature using all the data for Europe for the month of January 1996.

There is a low incidence of fog over snow or ice (Petterssen 1969). In fact, it is difficult for fog to develop over a snow surface, due to the difference between the saturation vapour pressure over ice and over water. As a consequence, sublimation usually occurs directly on the snow, before the air becomes saturated. According to Petterssen (1969) this effect is largest in the interval -10°C to -15°C. For temperatures below -40°C, fog amounts increase again and are frequent during such low temperature conditions when fog is composed entirely of ice crystals.

The frequency of occurrence of fog formed of ice crystals is still a matter of discussion. According to Vowinckel and Orvig (1970), low temperature fogs only form around settlements. On the other hand, Curry et al. (1990) claim that the presence of ice crystals in the lower troposphere is a common event in the Arctic polar night. These situations are associated with low visibility in the horizontal but with a good visibility in the vertical that often leads to the designation of "cloudless" ice-crystal precipitation. Since these events are more frequent during the polar night, they are difficult to observe, both from the surface or satellite. However, according to Curry et al. (1990, 1993), these lower tropospheric ice crystals are quite opaque to longwave radiation and might play a fundamental role on the radiative balance of the surface and the temperature profile of the lower troposphere during winter.

Since the prognostic cloud scheme permits mixed phase clouds, it should be able to handle realistically the behaviour of fog over ice or snow when the air temperature is below 0°C. To see how the mixed phase can reduce the frequency of fog, let's suppose that the temperature of the atmosphere at the lowest model level is -10°C. In the prognostic cloud scheme the atmosphere would need a moisture content of 1.65 g/kg to become saturated. However, if the cloud scheme had no mixed phase, it would only be necessary to have a moisture content of 1.59 g/kg to saturate the atmosphere.

Even if the temperature of the surface is the same as in the lowest model level, (which is unrealistic since surface inversions over snow are common in high latitudes in winter) the model's downward flux of moisture to the surface would prevent the model atmosphere from becoming saturated, leading to a moisture content of the lowest model level close to the saturation value over ice.

From the previous discussion it would be expected that the amount of fog should decrease with decreasing temperatures from 0°C to -40°C. Above 0°C the amount of fog should at some point also decrease with increasing temperatures. In fact a plot, based on observations, of the probability of occurrence of fog versus temperature in Petterssen (1969) shows both of these behaviours and a maximum value of the probability of occurrence of fog close to 0°C.

In fig. 25 the average liquid/ice water content versus the 2m temperature is shown for the model and the observations. This average is performed dividing the temperature in intervals of 2°C and uses all the observations over Europe for the period of January 1996, which is around 100000 observations. Within the range of temperatures that were actually measured, the general behaviour of the observations is close to the one reported by Petterssen (1969). The behaviour of the model in the range from -10°C to 10°C can be considered quite good when compared to the observations. The peak for both the observations and the forecasts is at -2°C and has a remarkably similar value of around 0.015 g/kg. Above 10°C the model values approach zero while the observations maintain an almost constant value between 0.0005 g/kg and 0.001 g/kg. This value probably corresponds to bad visibility due to dust and pollution.

Below -10°C the model produces more fog than it is observed. However, the number of observations and model events below -10°C is small and the amount of ice starts to be the dominant component of fog which makes the use of the relation proposed by Kunkel (1984) questionable. All this makes the results below -10°C not very reliable.

It is known, at least since Taylor (1917), that light winds are conducive to fog formation over land (e.g. radiation fog) and there is a consensus that the frequency of occurrence of fog decreases with increasing wind speed. However, there is a certain degree of controversy about the role, in the development of fog, of the turbulent mixing at low wind speeds (e.g. Gerber 1981; Welch et al. 1985).

Some authors (e.g. Roach et al. 1976) believe that very low wind speeds contribute to fog generation while others (e.g. Rodhe 1962; Gerber 1981; Welch et al. 1985) think that the role of turbulent mixing is fundamental for the development of fog, and that therefore very low wind speeds do not produce enough mixing for fog development.

In fig. 26 the average liquid/ice water content versus the 10 m wind speed is shown. This average is performed dividing the wind speed in intervals of 1 m/s and uses all the observations over Europe for January 1996. A decrease of liquid/ice water with increasing wind can be clearly seen, both for the model and the observations. In that respect the model and the observations have a similar behaviour. Also the peak values of liquid/ice water both for the model and the observations are very similar and around 0.0105 g/kg.

However, while in the observations the two highest values for liquid/ice water are at 0 m/s and 1m/s, in the forecast these peak values correspond to wind speeds of 1 m/s and 2 m/s. Actually in the model the peak value at 2m/s is followed by a decrease of the average liquid/ice water with decreasing wind speed. On the observations the liquid/ice water increases until it reaches its peak value at 0 m/s.

In this case the observations seem to favour the idea that very low wind speeds help fog to form while the forecasts seem to support the belief that very low wind speeds will decrease the amount of fog. However, both the observations and the model may be correct if the fact that the height of the observer is lower than the height of the lowest model level (around 30m) is taken into account. These results tell us that very low wind speeds might be good for fog formation close to the surface but do not always produce enough mixing for fog to grow up to 30m.

At wind speeds above 4 m/s the results show that the model underestimates the amount of liquid/ice water. However, most of the fog events in the model are concentrated in the range between 0 m/s and 4 m/s while in the observations they are more spread over a wider wind speed range. These results are probably related to the model tendency to underestimate the wind speed in stable situations. Above 12 m/s the amount of liquid/ice water in the model is negligible and its value is an artificial minimum value imposed by the parametrization. In the observations the amount of liquid/ice water is still a significant value which means that there is a relatively low average horizontal visibility. At these wind speeds, low visibility is not due to fog but is probably associated with mid-latitude weather systems (e.g. precipitation).

6. Conclusions

The one-column version of the ECMWF model was used to simulate a well documented radiation fog case. A detailed analysis of how the model simulates the main mechanisms of fog generation and dissipation in radiation fog was presented. The comparison between the simulated and the observed visibility shows that the onset of fog, the lowest values of visibility and the dissipation stage are properly simulated.

From analysing the tendencies from the different parametrized physical processes it can be concluded that the subtle balances between the various parametrized processes necessary to have a good fog forecast are actually achieved. The analysis of the Clausius-Clapeyron diagram for the model's lowest model level provides a better understanding of the fog's evolution and shows the role of longwave atmospheric cooling in radiation fog. This study shows that, although the thermodynamic state of the lowest model layer always evolves in time along a mixing line during the first hours of the simulation or until the onset of fog, it needs radiative cooling to change T without changing q in order to reach saturation.

A climatology of the model's fog was produced using data from the ECMWF Re-Analysis (ERA). The comparison between these results and fog climatological data showed that the model with the prognostic cloud scheme is able to reproduce most of the major fog areas, particularly over the ocean. One exception is the lack of simulated fog at the west coast of continents. This seems to be related to a poor representation of stratocumulus and to difficulties of the model in parametrizing the processes that control the evolution and interaction between fog and low stratus.

High resolution (T213L31) 60 and 72 hour fog forecasts for Europe have been discussed for the period of September 1995 to January 1996. The forecasts were compared with synoptic observations of visibility and it was shown that the model reproduces some of the major areas of fog and mist in Europe. The diurnal cycle is reproduced reasonably well by the model by producing more fog at 0 UTC than at 12 UTC, but the amount of fog at 12UTC is too low when compared to the observations.

The number of situations where the visibility is between 2 km and 11 km is largely underestimated by the model when compared with the observations. This might be due to other physical factors like rain, drizzle, snow, dust or atmospheric pollutants that limit the horizontal visibility and to problems that might still exist in the parametrization of fog

Time series of liquid/ice water content from the observations and T213L31 forecasts (30, 36, 42 and 48 hour) were also analysed for all available surface stations in Europe and for two smaller areas in Europe. The results are good particularly at 0 UTC and 6 UTC. During the day (12 UTC) the fog in the model is usually underestimated.

The corresponding time series for the 2 m temperature shows an almost constant negative temperature bias of around -4°C. It was shown that the model is always slightly closer to saturation than the observations and this might help the model to produce fog. However, there is no direct correlation between the cold bias and the performance of the fog forecast.

A plot of the average liquid/ice water content versus the 2 m temperature showed that the model reproduces the observed behaviour of fog as a function of temperature. The amount of fog reaches a peak value at a temperature close to 0°C (around -2°C) and decreases with increasing or decreasing temperatures. Actually, the behaviour of the model in the range from -10°C to 10°C can be considered quite good when compared to the observations. A plot of the average liquid/ice water content versus the wind speed at 10m showed that the model reproduces the observations with a decrease of liquid/ ice water with increasing wind speed.

As discussed in the introduction, the subtle balances between the various parametrized processes required for fog physics and also the results discussed here suggest that the monitoring and study of fog in the model will provide impetus to improvements of the model parametrization schemes (e.g. the interaction between fog and low stratus).

Acknowledgments

I would like to thank Tony Hollingsworth, Adrian Simmons, Pedro Viterbo and Peter Duynkerke for reading a draft version of this paper and providing useful comments. Special thanks to Martin Miller for commenting on the paper, to Stephen Klein for providing the observed climatology data and in particular to Anton Beljaars for providing invaluable guidance. The fog verification maps over Europe presented in section 5 were developed together with Bruno David and Andreas Lanzinger helped with the time series plots.

References

Ballard, S.P., B.W. Golding and R.N.B. Smith, 1991: Mesoscale Model Experimental Forecasts of the Haar of Northeast Scotland. Mon. Weather Rev., 119, 2107-2123.

Barry, R.G., 1981: Mountain Weather and Climate. Methuen, 313 pp.

Beljaars, A.C.M. and Holtslag, A.A.M. 1991: Flux parametrization over land surfaces for atmospheric models, J. Appl. Meteor., 30, 327-341.

Beljaars, A.C.M. and Betts, A.K. 1993: Validation of the boundary layer representation in the ECMWF model, ECMWF Seminar proceedings 7-11 September 1992, Validation of models over Europe, Vol II, 159-196.

Bergot, T. and D. Guedalia, 1994: Numerical Forecasting of Radiation Fog. Part I: Numerical Model and Sensitivity Tests. Mon. Weather Rev., 122, 1218-1230.

Bott, A., U. Sievers and W. Zdunkowski, 1990: A Radiation Fog Model with a Detailed Treatment of the Interaction between Radiative Transfer and Fog Microphysics. J. Atmos. Sci., 47, 2153-2166.

Brown, R. and W.T. Roach, 1976: The physics of radiation fog. II- A numerical study. Quart. J. Roy. Meteor. Soc., 102 335-354.

Campana, K.A., 1990: Radiation and Cloud Parameterization at the National Meteorological Center. Proc. ECMWF/ WCRP Workshop on Clouds, Radiative Transfer and the Hydrological Cycle. 12-15 November 1990, ECMWF, Reading, United Kingdom, 313-340.

Cotton, W.R. and R.A. Anthes, 1989: Storm and Cloud Dynamics. Academic Press, 880 pp.

Curry, J.A., F.G. Meyer, L.F. Radke, C.A. Brock and E.E. Ebert, 1990: Occurrence and Characteristics of Lower Tropospheric Ice Crystals in the Arctic. Int. J. Climatology, 10, 749- 764.

Curry, J.A., J.L. Schramm and E.E. Ebert, 1993: Impact of Clouds on the Surface Radiation Balance of the Arctic Ocean. Meteor. Atmos. Phys., 51, 197-217.

Duynkerke, P.G., 1991: Radiation fog: a comparison of model simulation with detailed observations. Quart. J. Roy. Meteor. Soc., 117, 1207-1224.

Fisher, E.L. and P. Caplan, 1963: An Experiment in Numerical Prediction of Fog and Stratus. J. Atmos. Sci., 20, 425-437.

Gerber, H.E., 1981: Microstructure of a radiation fog. J. Atmos. Sci., 38, 454-458.

Gibson, J.K, Kallberg, S. Uppala, A. Hernandez, A. Nomura and E. Serrano, 1997: 1. ERA Description. ECMWF Re-Analysis, Project Report Series, July 1997, ECMWF, Reading, United Kingdom, pp. 72.

Golding, B.W., 1993: A Study of the Influence of Terrain on Fog Development. Mon. Weather Rev., 121, 2529-2541.

Grandin, G., 1983: A one-dimensional PBL model with a sub-grid scale condensation scheme for stratiform clouds and fogs. Report 72, Uppsala University, Uppsala, Sweden.

Houze, R.A., Jr., 1993: Cloud Dynamics. Academic Press, 570 pp.

Jakob, C., 1995: The impact of the new cloud scheme on ECMWFs Integrated Forecasting System (IFS). Proc. of ECMWF/GEWEX Workshop on Modelling, Validation and Assimilation of Clouds, November 1994, ECMWF, Reading, United Kingdom, 277-294.

Klein, S.A. and D.L. Hartmann, 1993: The Seasonal Cycle of Low Stratiform Clouds. J. Climate, 6, 1587-1606.

Kvamsto, N.G., 1993: Synoptic Cloudiness Validation in the ECMWF Model. ECMWF Technical Memorandum No.193. ECMWF, Reading, United Kingdom, 30 pp.

Kunkel, B.A., 1984: Parameterization of Droplet Terminal Velocity and Extinction Coefficient in Fog Models. J. Clim. Appl. Meteor., 23, 34-41.

Lott, F. and Miller, M.J. 1997: A new subgrid-scale orography parametrization: Its formulation and testing, Quart. J. Roy. Meteor. Soc., 123, 101-127.

Louis, J.F., Tiedtke, M. and Geleyn, J.F. 1982: A short history of the operational PBL-parameterization at ECMWF, Workshop on boundary layer parameterization, November 1981, ECMWF, Reading, England.

Miller, M., M. Hortal and C. Jakob, 1995: A major operational forecast model change. ECMWF Newsletter Number 70, Summer 1995, ECMWF, Reading, United Kingdom, 2-8.

Moeng, C.H., 1993: Stratus-Topped Boundary-Layer Parameterization in Large-Scale Models. Proc. ECMWF/GCSS Workshop on Parametrization of the cloud topped boundary layer. 8-11 June 1993, ECMWF, Reading, United Kingdom, 259-278.

Morcrette, J.-J., 1990: Impact of changes in the radiation transfer parametrization plus cloud optical properties in the ECMWF model, Mon. Wea. Rev., 118, 847-873.

Musson-Genon L., 1987: Numerical simulation of a fog event with a one-dimensional boundary layer model. Mon. Weather Rev., 117, 29-39.

Oliver, D.A., W.S. Lewellen, and G.G. Williamson, 1978: The interaction between turbulent and radiative transport in the development of fog and low-level stratus. J. Atmos. Sci., 35, 301-316.

Petterssen, S., 1969: Introduction to Meteorology. Third edition, McGraw-Hill, 333 pp.

Pilie, R.J., E.J. Mack, C.W. Rogers, U. Katz and W.C. Kocmond, 1979: The Formation of Marine Fog and the Development of Fog-Stratus Systems along the California Coast. J. Appl. Meteor., 18, 1275-1286.

Ratisbona, L.R, 1976: The climate of Brazil. Climates of Central and South America, World Survey of Climatology. Ed. W. Schwerdtfeger, Elsevier Scientific, vol.12, 219-269.

Reiff, J., 1987: Forecasting boundary layer clouds and fog: a review on operational numerical models. Proc. of the International Symposium on Mesoscale Analysis and Forecasting, 17-19 August 1987, Vancouver, Canada. Published by ESA, ESTEC, Noordwijk, The Netherlands, 407-414.

Ritchie, H., C. Temperton, A.J. Simmons, M. Hortal, T. Davies, D. Dent, and M. Hamrud, 1995: Implementation of the Semi-Lagrangian method in a high resolution version of the ECMWF forecast model. Mon. Wea. Rev., 123, 489-514.

Roach, W.T., R. Brown, S.J. Caughey, J.A. Garland, and C.J. Readings, 1976: The physics of radiation fog: I - A field study. Quart. J. Roy. Meteor. Soc., 102, 313-333.

Rodhe, B., 1962: The effect of turbulence on fog formation. Tellus, 14, 49-86.

Slingo, J.M., 1987: The Development and Verification of a Cloud Prediction Scheme in the ECMWF Model. Quart. J. Roy. Meteor. Soc., 113, 899-927.

Smith, R.N.B, 1990: A scheme for predicting layer clouds and their water content in a general circulation model. Quart. J. Roy. Meteor. Soc., 116, 435-460.

Stull, R.B., 1995: Meteorology today for Scientists and engineers, a technical companion book. West Publishing Company, 385 pp.

Sundqvist, H., 1988: Parametrization of condensation and associated clouds in models for weather prediction and general circulation simulation. In Physically-Based Modelling and Simulation of Climate and Climate Change, M.E. Schlesinger Ed., Kluwer, 433-461.

Taylor, G.I, 1917: The formation of fog and mist. Quart. J. Roy. Meteor. Soc., 43, 241-268.

Tiedtke, M. 1989: A comprehensive mass flux scheme for cumulus parametrization in large-scale models, Mon. Wea. Rev., 117, 1779-1800.

Tiedtke, M., 1993: Representation of Clouds in Large-Scale Models. Mon. Weather Rev., 121, 3040-3061.

Tremant, M., 1989: The Forecasting of Sea Fog. Met. Mag., 118, 69-75.

Turton, J.D. and R. Brown, 1987: A comparison of a numerical model of radiation fog with detailed observations. Quart. J. Roy. Meteor. Soc., 113, 37-54.

Vowinckel, E. and S. Orvig, 1970: The climate of the North Polar basin. Climates of the Polar regions, World Survey of Climatology. Ed. S. Orvig, Elsevier Scientific, Vol.14, 129- 226.

Viterbo, P. and Beljaars, A.C.M. 1995: An improved land surface parametrization scheme in the ECMWF model and its validation, J. Clim., 8, 2716-2748.

Viterbo, P., A.C.M. Beljaars, J-F Mahfouf, and J. Teixeira, 1998: The role of soil water freezing in the interaction of the surface with the stable boundary layer. To be submitted.

Warren, S.G., C.J. Hahn, J. London, R.M. Chervin and R.L. Jenne, 1986: Global Distribution of Total Cloud Cover and Cloud Type Amounts over Land. NCAR Technical Note NCAR/TN-273+STR. NCAR, Boulder, United States. 29 pp, plus 200 maps.

Warren, S.G., C.J. Hahn, J. London, R.M. Chervin and R.L. Jenne, 1988: Global Distribution of Total Cloud Cover and Cloud Type Amounts over the Ocean. NCAR technical note NCAR/TN-317+STR. NCAR, Boulder, United States. 42 pp, plus 170 maps.

Welch, R.M, M.G. Ravichandran, and S.K. Cox, 1986: Prediction of quasi-periodic oscillations in radiation fogs. Part I: comparison of simple similarity approaches. J. Atmos. Sci., 43, 633-651.

W.M.O., 1966: International Meteorological Vocabulary, 275 pp.

Zdunkowski, W.G. and A.E. Barr, 1972: A Radiative Conductive Model for the Prediction of Radiation Fog. Bound. Layer Meteor, 2, 152-177.

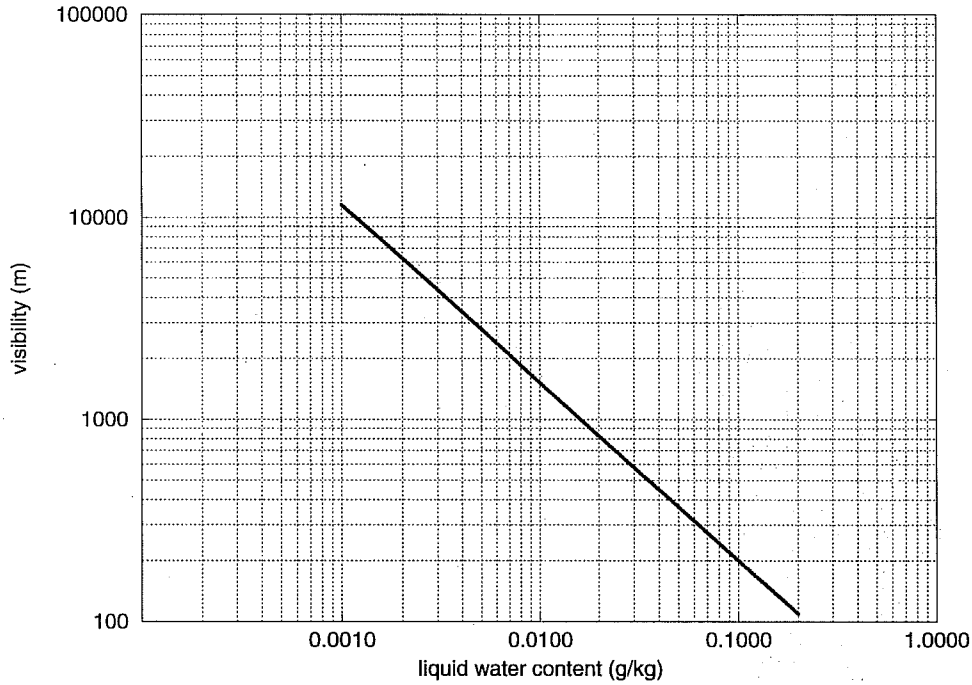

Fig. 1 The liquid water content versus visibility according to the relation proposed by Kunkel (1984).

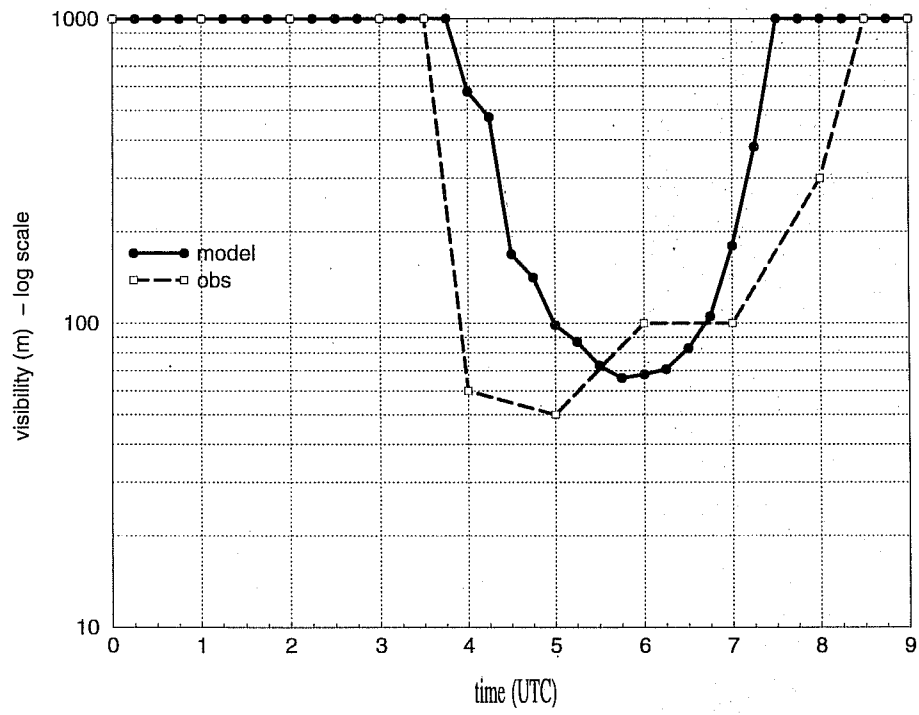

Fig. 2 The time evolution of the simulated visibility at the lowest model level together with the visibility observations from the Cabauw tower at the 30 m level.

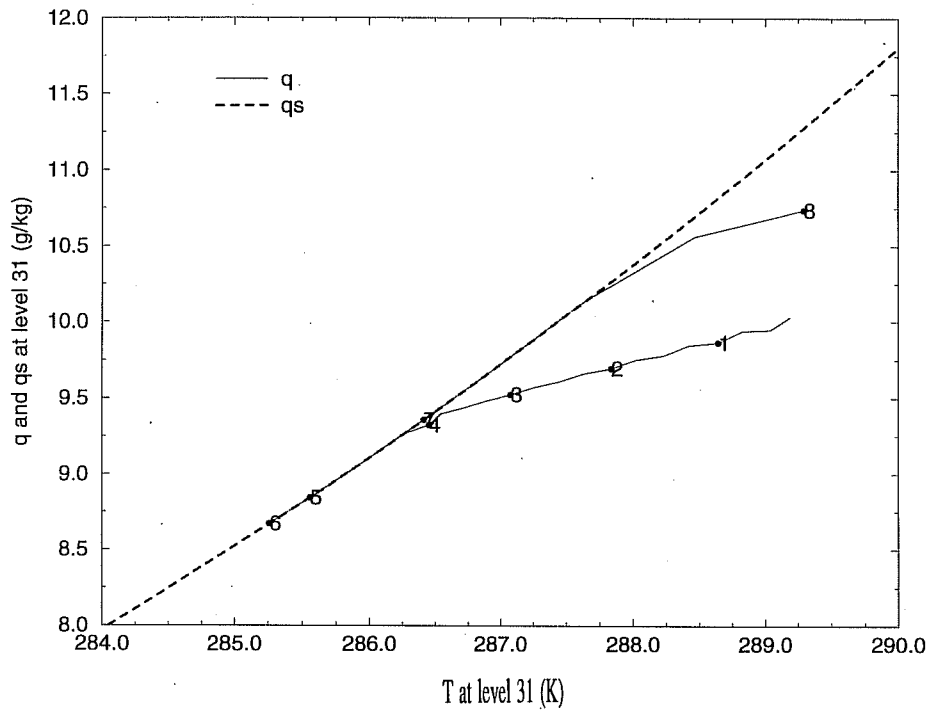

Fig. 3 The Clausius-Clapeyron diagram for the model's lowest model level, with q and q_s as a function of T. The dots and the numbers represent the hours of simulation (in UTC).

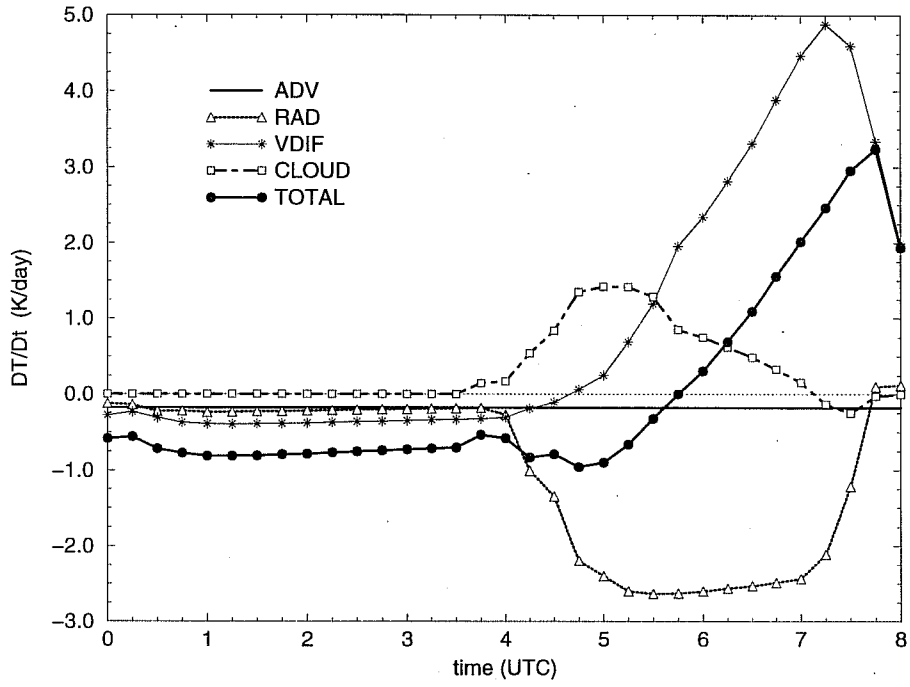

Fig. 4a The lowest model level temperature tendencies (in K/day), produced by the different physical processes.

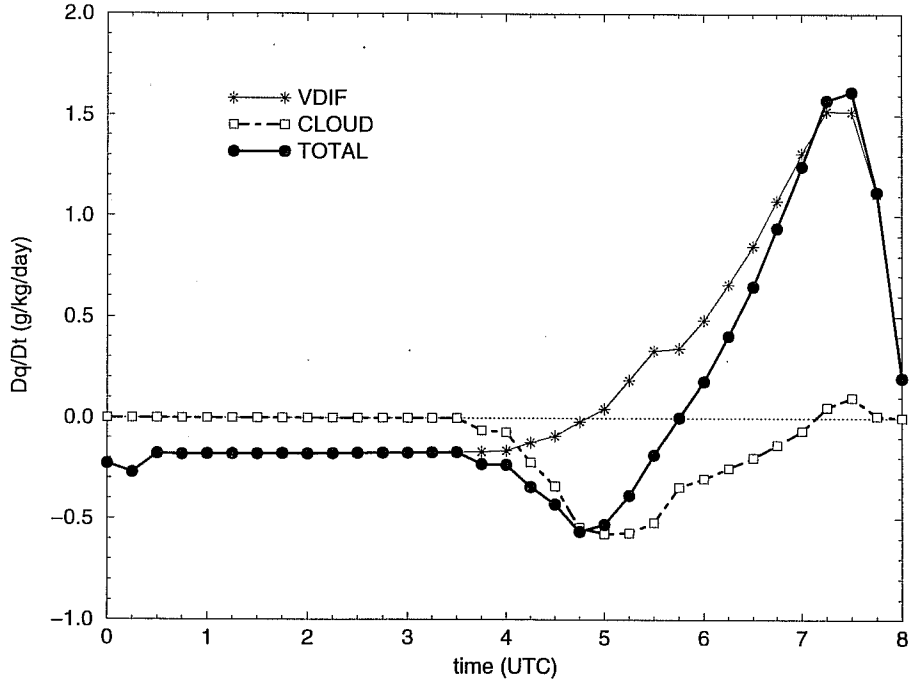

Fig. 4b The lowest model level specific humidity tendencies (in g/kg/day), produced by the different physical processes.

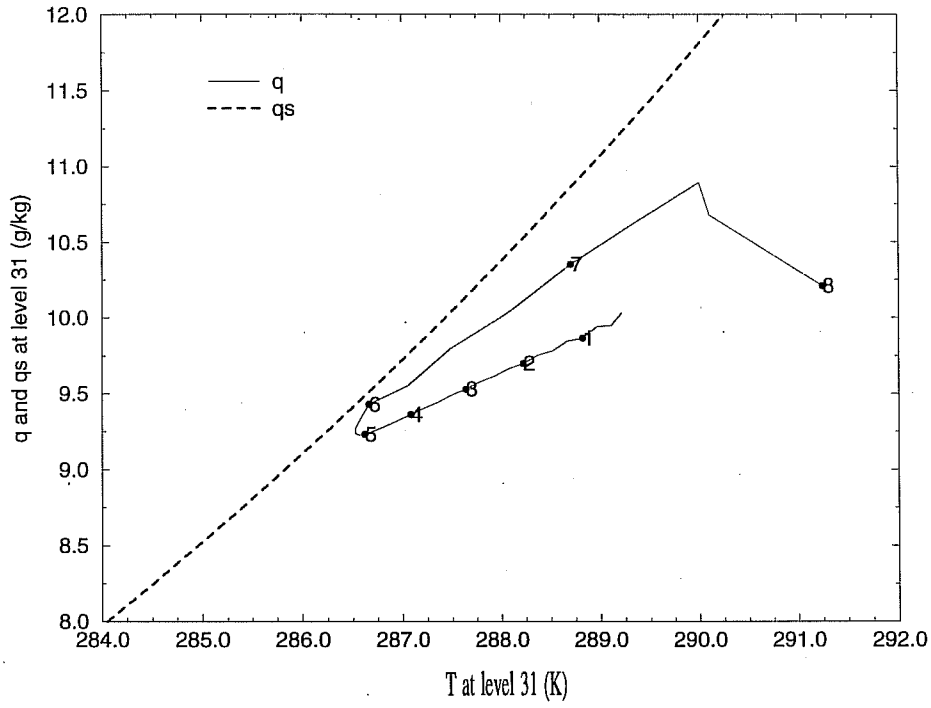

Fig. 5 As in fig. 3 but for a sensitivity experiment with the longwave atmospheric cooling switched off.

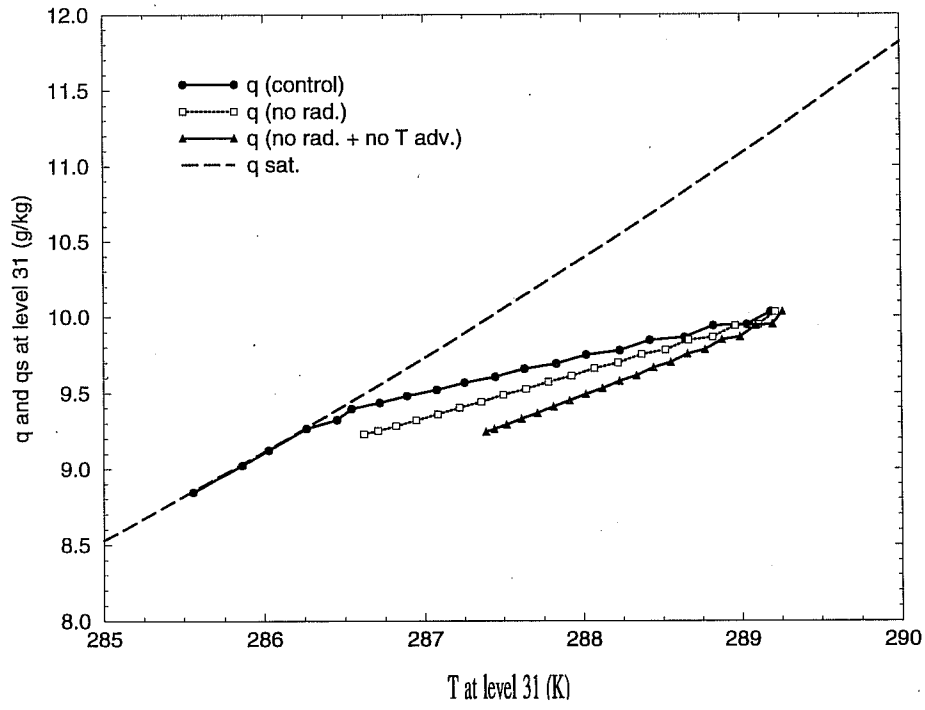

Fig. 6 Clausius-Clapeyron diagram, of the lowest model level, for the first 5 hours of 3 different experiments: control, control without radiative cooling of the atmosphere and control without radiative cooling of the atmosphere and horizontal cold advection.

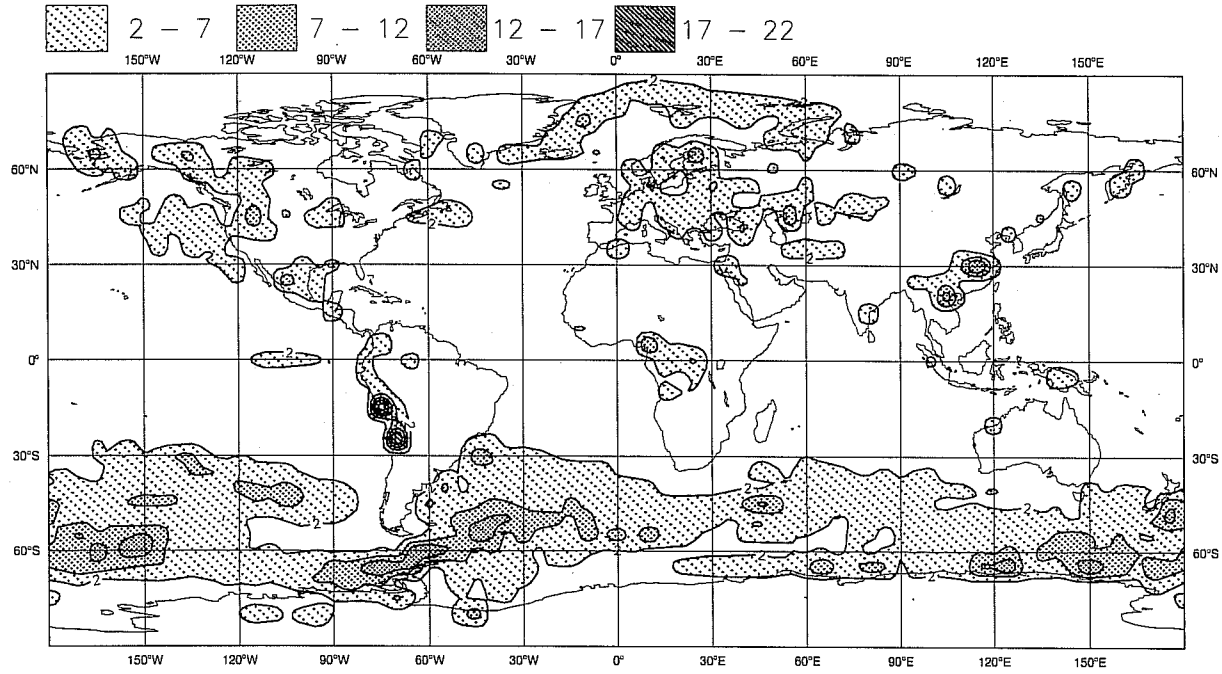

Fig. 7 The model's climatology of the frequency of occurrence of fog, for the December- January-February (DJF) period. To produce the fog climatology, 5 years of data from the ECMWF Re-Analysis (ERA) were analysed, from 1985 to 1989. The daily 6, 12, 18 and 24 hour forecasts were used. The first contour is at 2% and the contour interval is 5% for both plots.

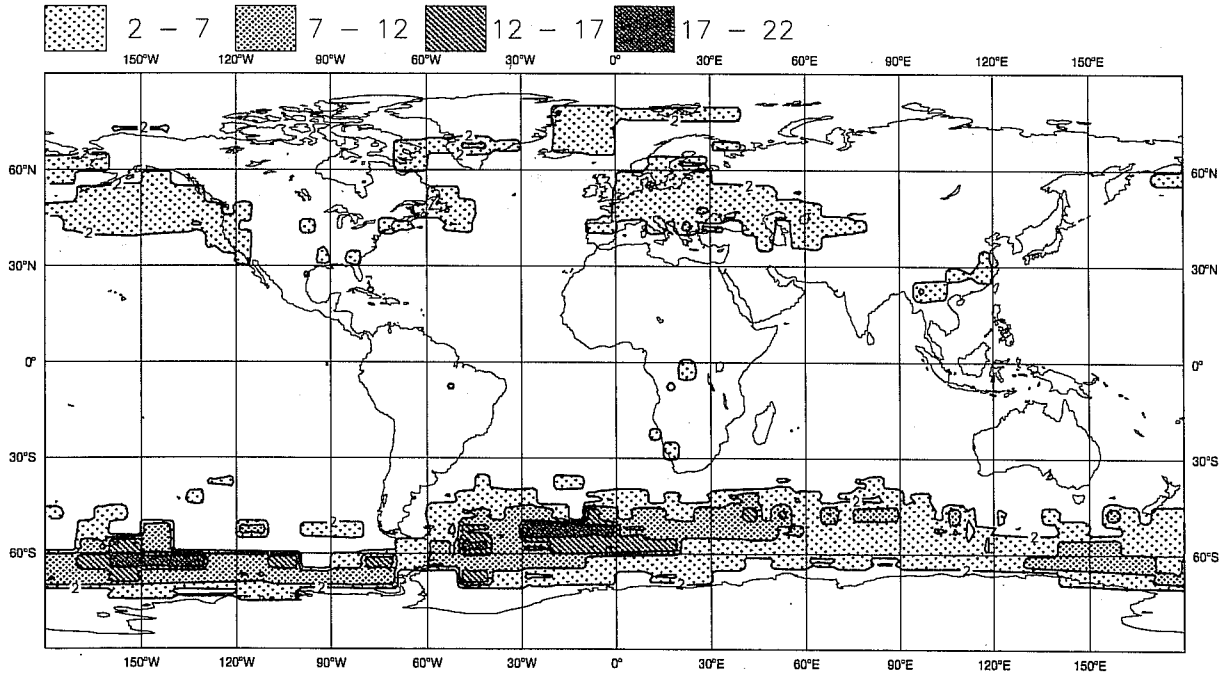

Fig. 8 The observed frequency of occurrence of "sky obscured" due to fog taken from the cloud climatology of Warren et al. (1986, 1988) for the DJF period. This climatology is based on surface observations, either ships or land stations. The climatology results represent averages of 30 (1951-1981) years of data for the oceans and 10 (1971-1981) years for the land areas. The first contour is at 2% and the contour interval is 5% for both plots.

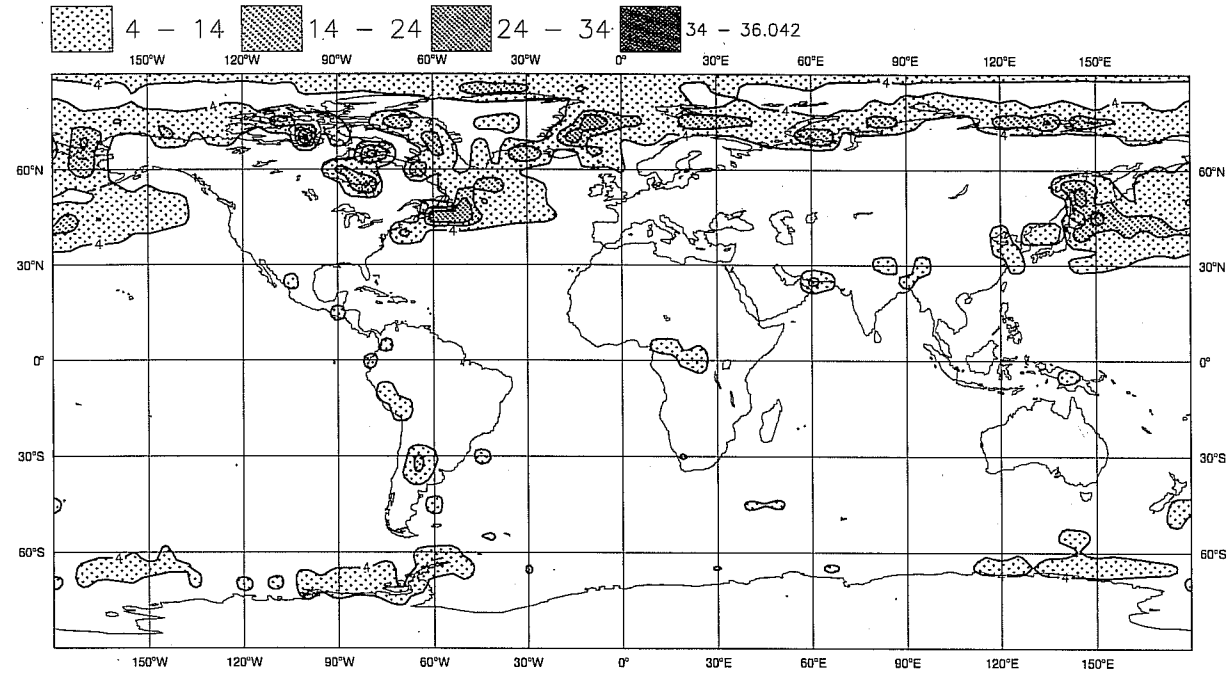

Fig. 9 As in fig.7 but for the June-July-August (JJA) period. The first contour is at 4% and the contour interval is 10%.

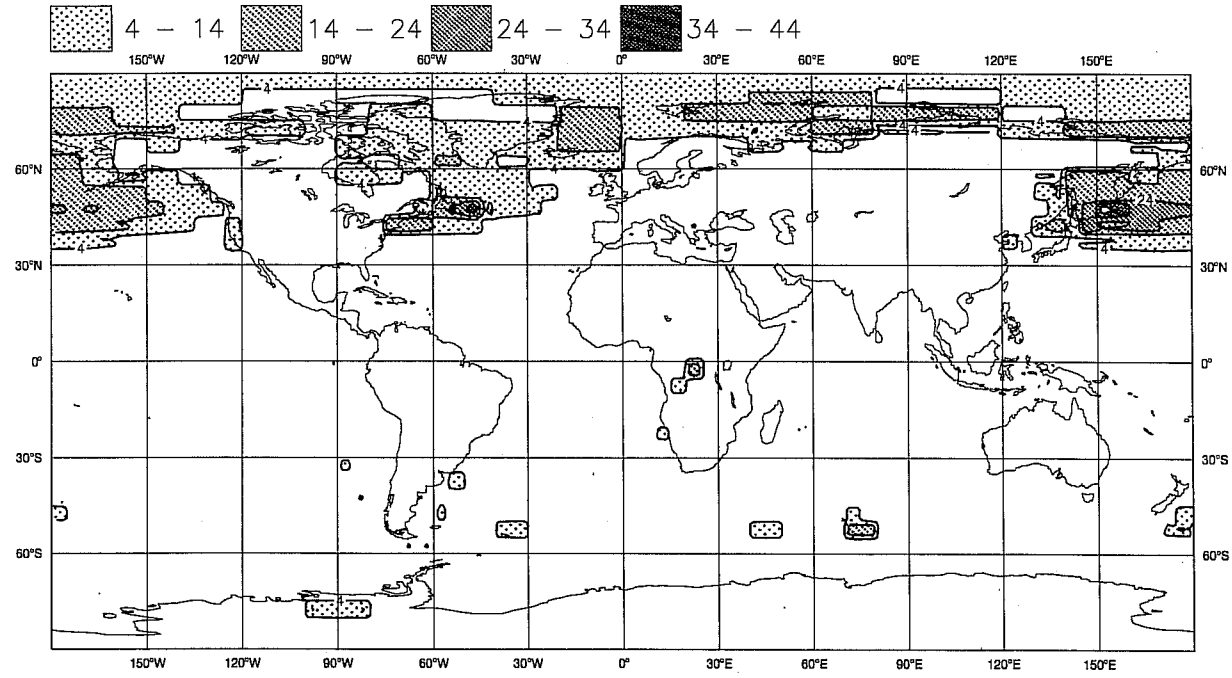

Fig. 10 As in fig. 8 but for the JJA period. The first contour is at 4% and the contour interval is 10%.

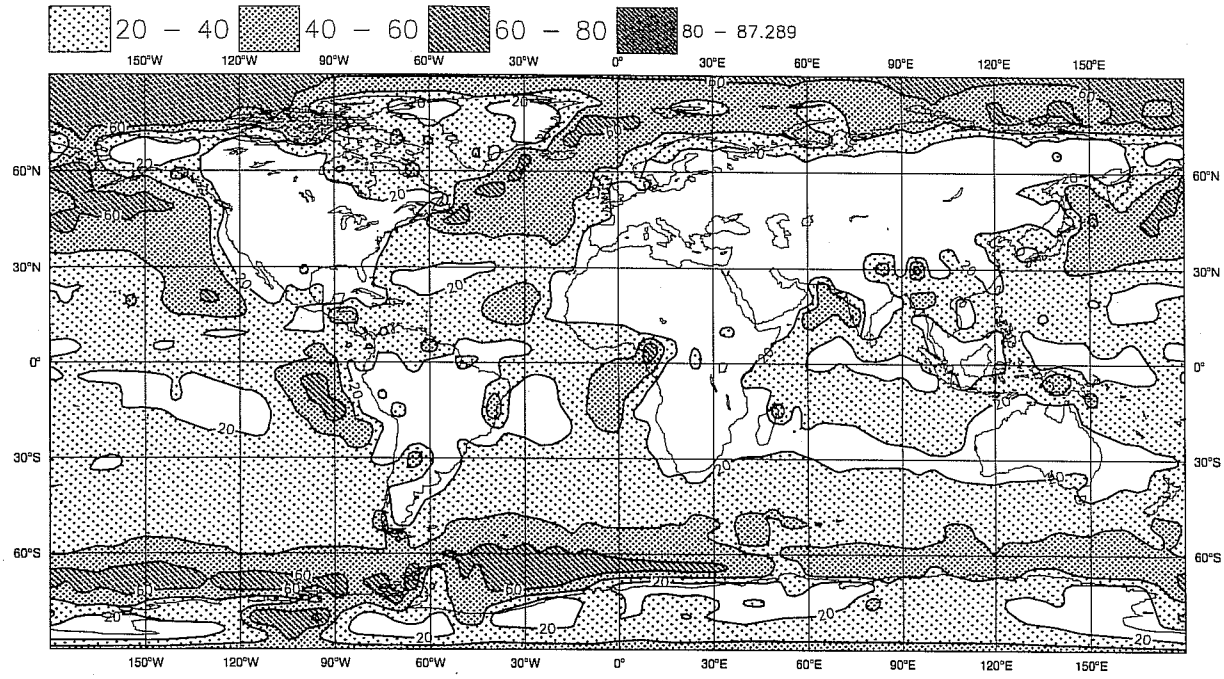

Fig. 11 The global distribution of low cloud cover produced by ERA for the period of June- July-August of 1985 to 1990. The daily 6, 12 18 and 24 hour forecasts were used. The first contour is at 20% and the contour interval is 20%.

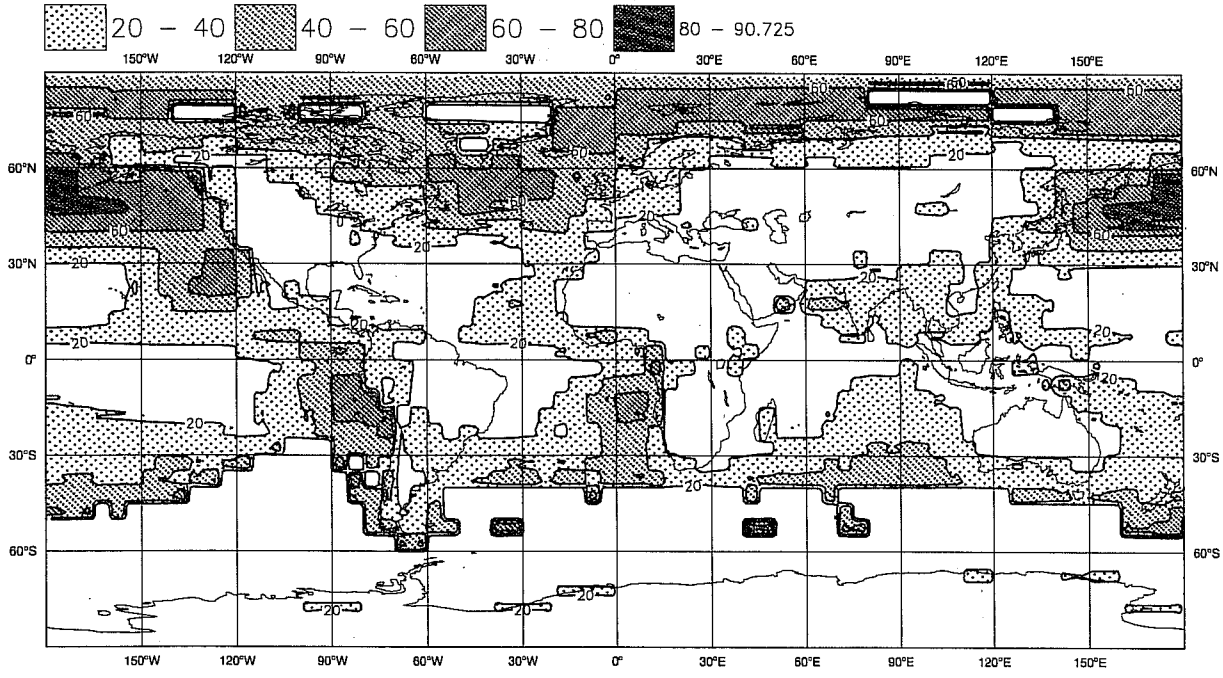

Fig. 12 The observed climatology of low stratus distribution (taken from Warren et al., 1986, 1988) for the JJA period. The first contour is at 20% and the contour interval is 20%.

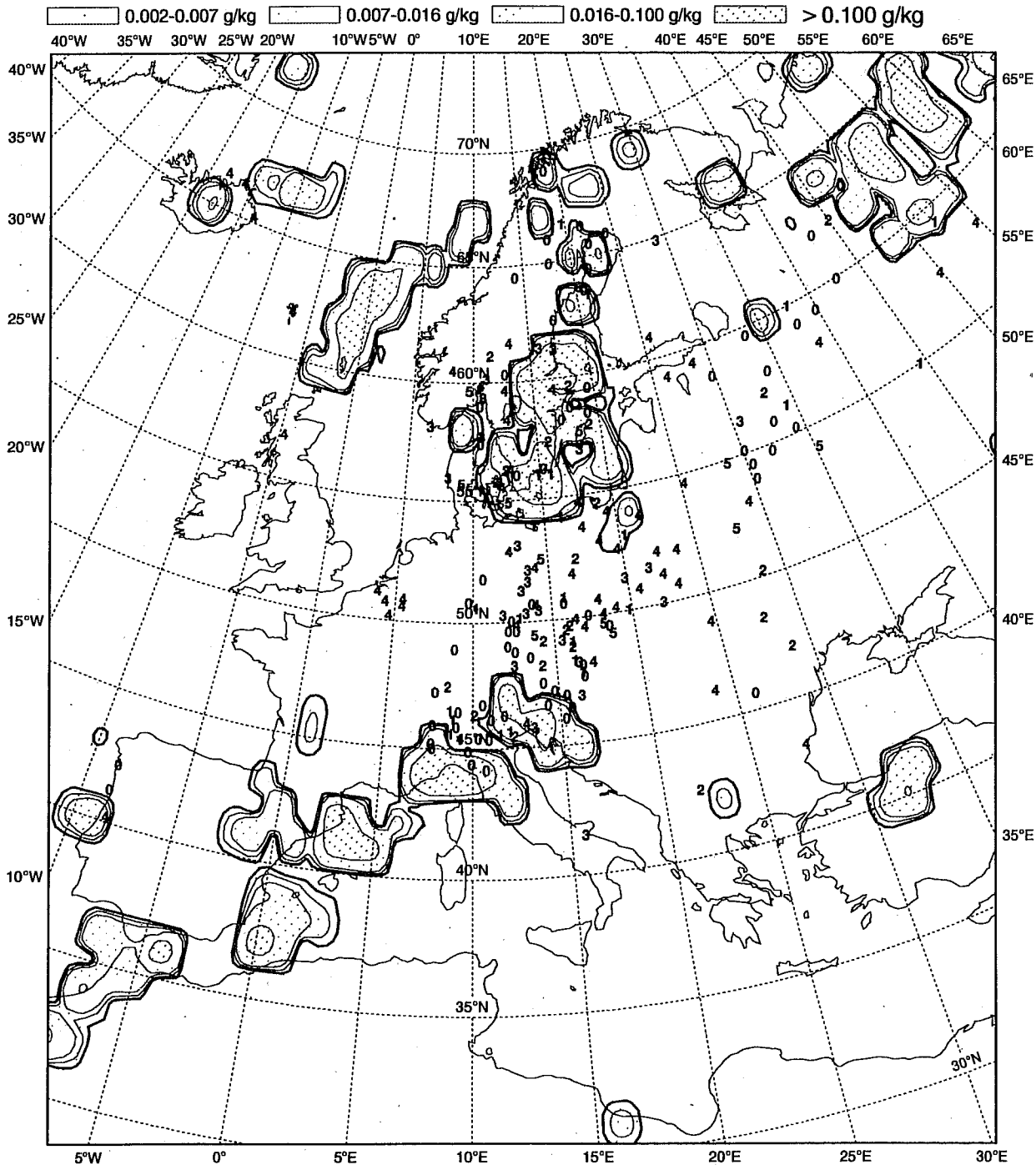

Fig. 13 The 60 hour forecasts of liquid/ice water content at the lowest model level, together with the visibility reported by the synop stations. Only the values from the stations that report visibility less than 6 km are shown. The number 0 means that the station is reporting values between 0 and 1 km of visibility and so on up to number 5. The liquid water contours are 0.002, 0.007, 0.016 and 0.1 g/kg. These values correspond roughly to values of horizontal visibility of 6 km, 2 km, 1 km and 200 m respectively (Kunkel 1984). The verification time is 0 UTC of 5 October 1995.

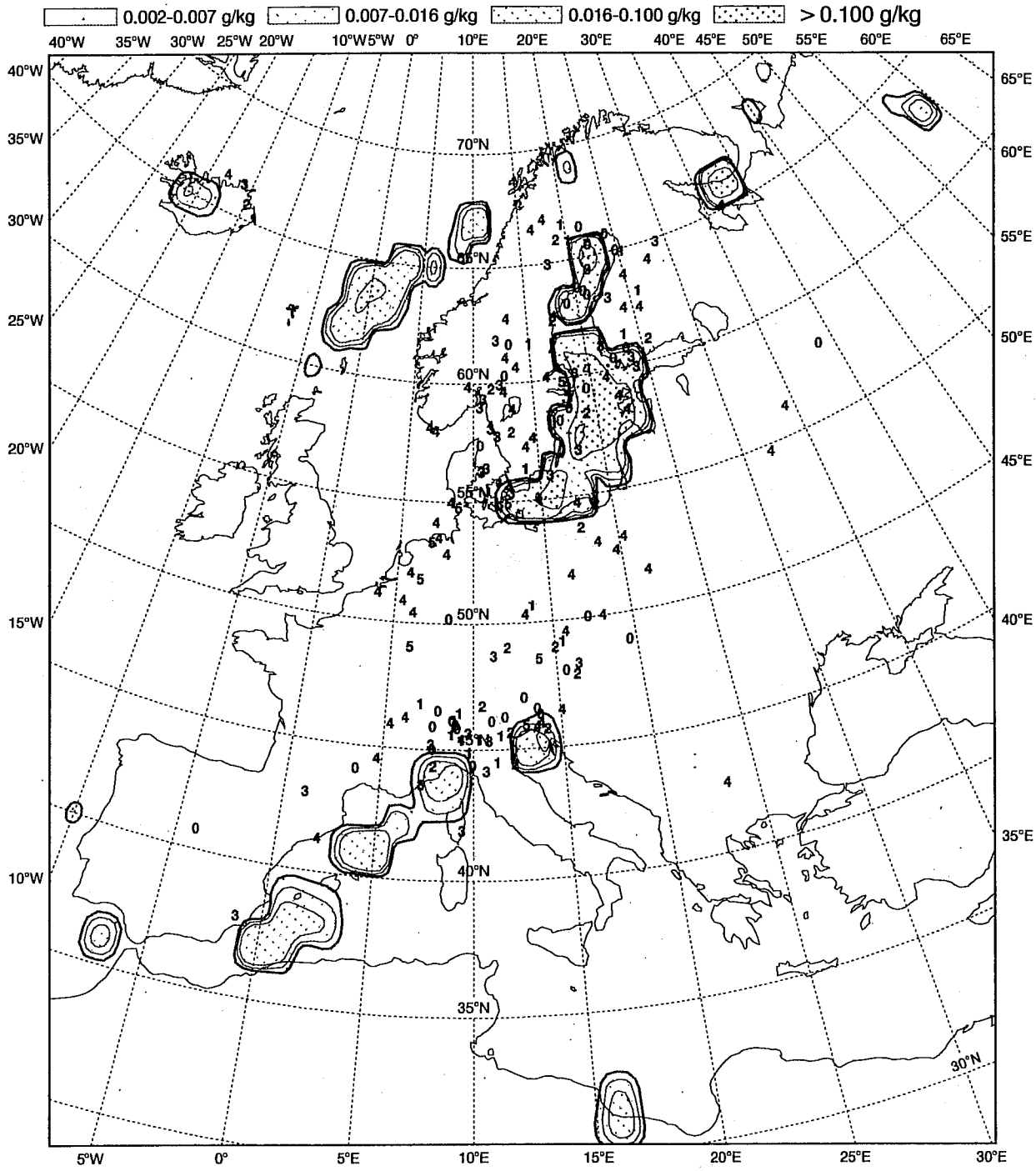

Fig. 14 As in fig. 13 but for the 72 hour forecast verifying at 12 UTC.

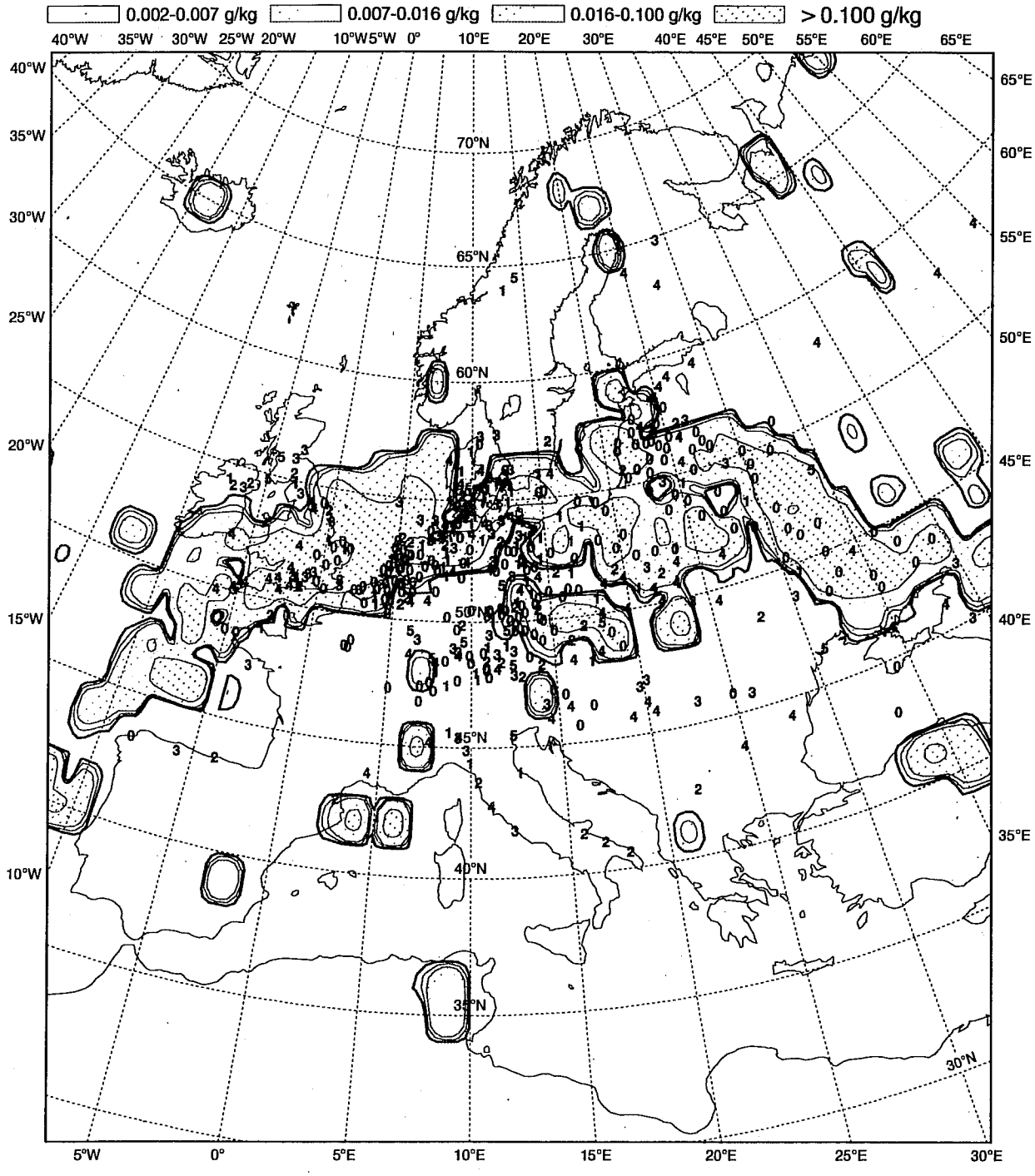

Fig. 15 As in fig.13 but for 13 October 1995.

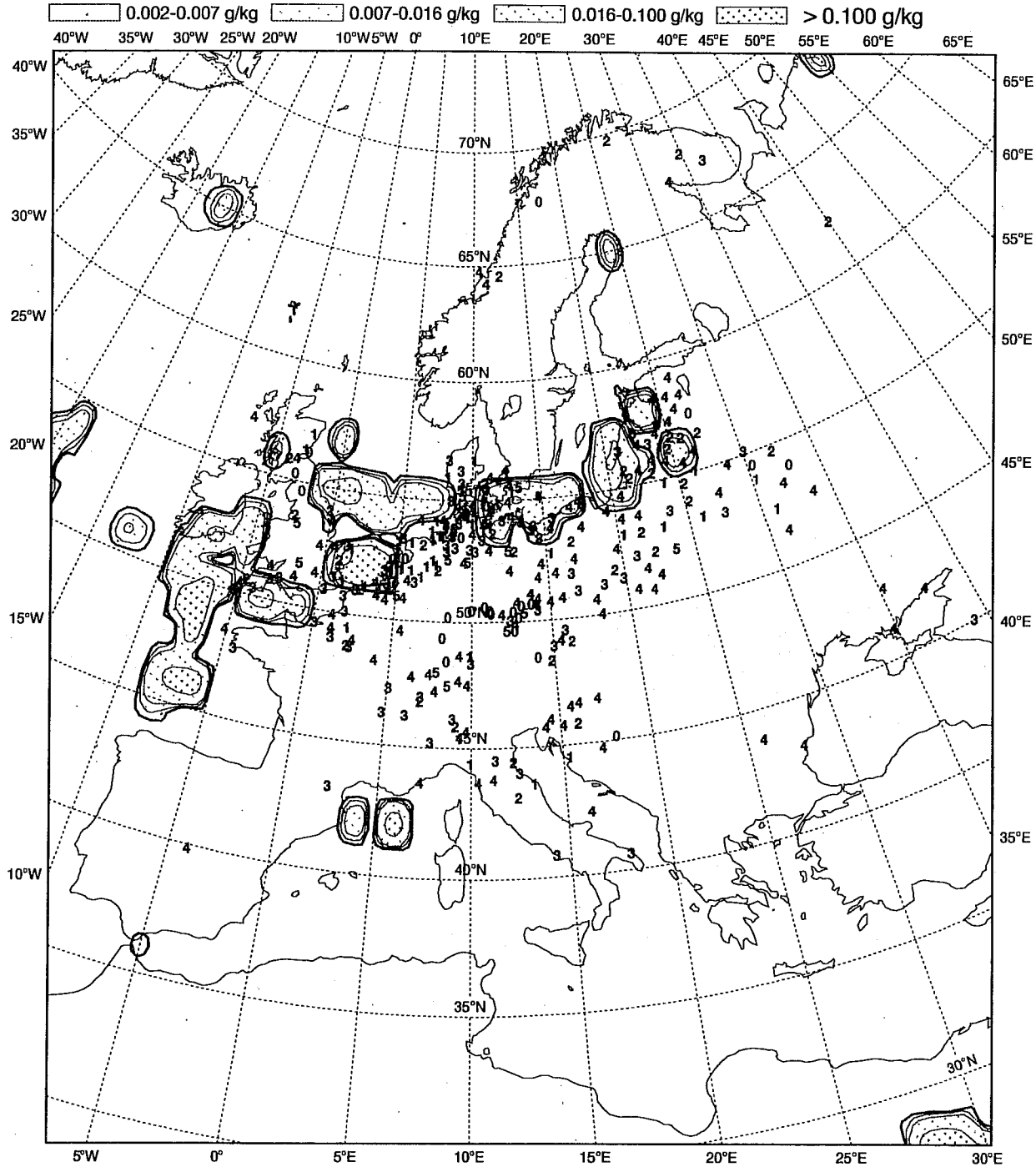

Fig. 16 As in fig.14 but for 13 October 1995.

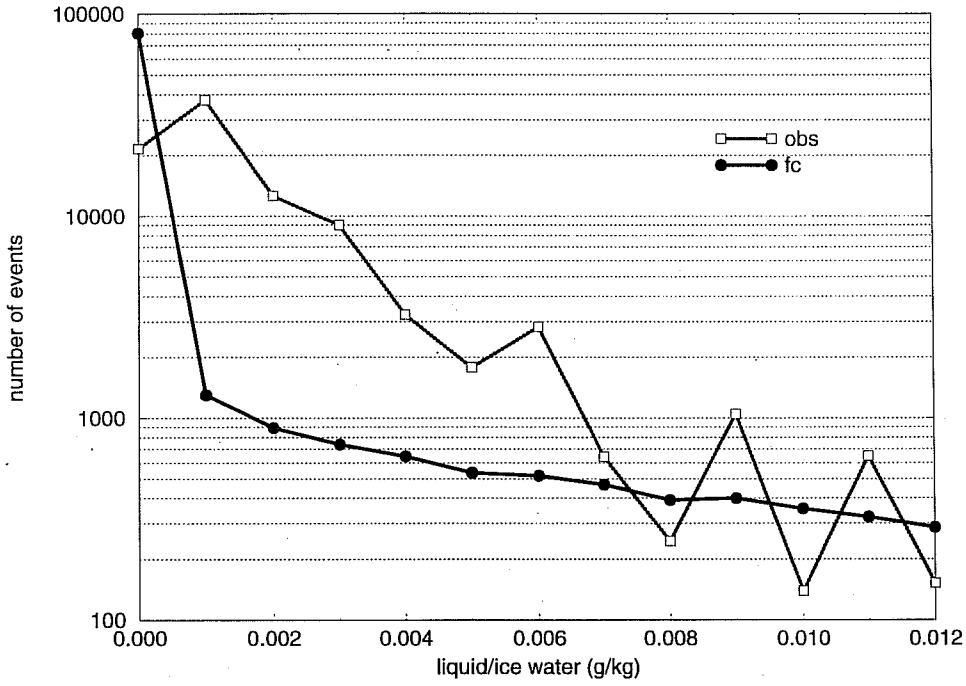

Fig. 17 The distribution of the number of fog events (observations and forecasts) for different values of liquid/ice water content. It uses the 30, 36, 42 and 48 hour forecasts and the synop observations for Europe for January 1996. The total number of events (including "fog" and "no fog" events) is around 100000. The observed visibility is converted to liquid/ice water content. The number of events is distributed in intervals of 0.001 g/kg of liquid/ice water content, except for the first interval that is from 0 g/kg to 0.0005 g/kg.

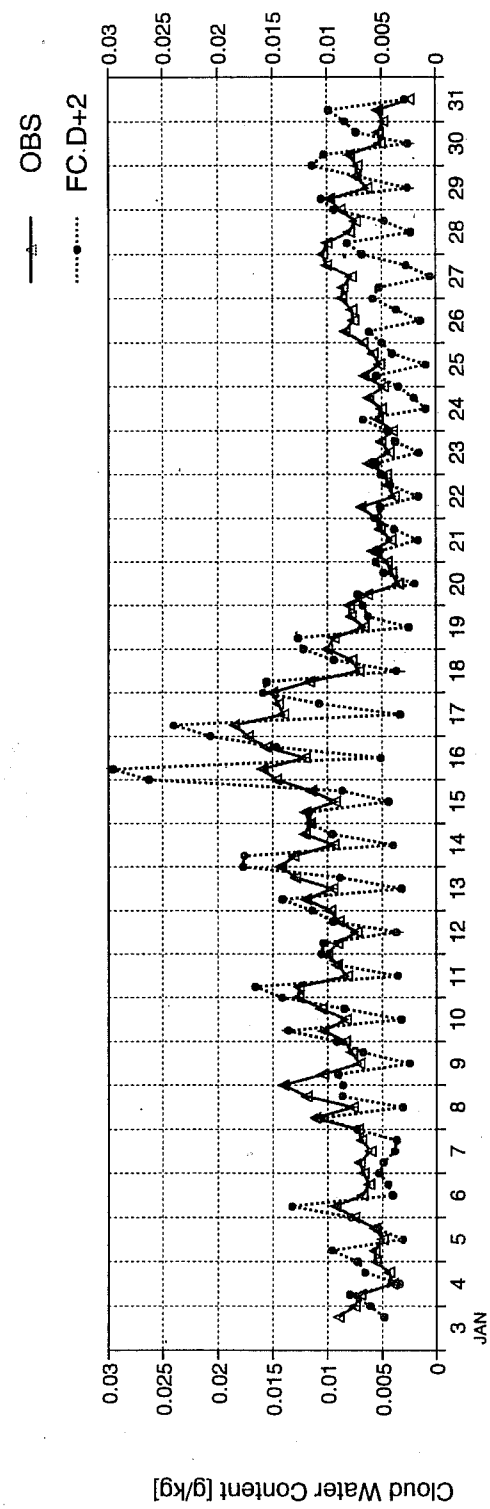

Fig. 18 Time series of liquid/ice water content for the synop observations and forecasts (30, 36, 42 and 48 hour) for Europe. It uses the 30, 36, 42 and 48 hour forecasts and synop observations for January 1996. The total number of observations is around 100000. The relation between visibility and liquid water content proposed by Kunkel (1984) is used to convert the observed visibility to liquid/ice water content.

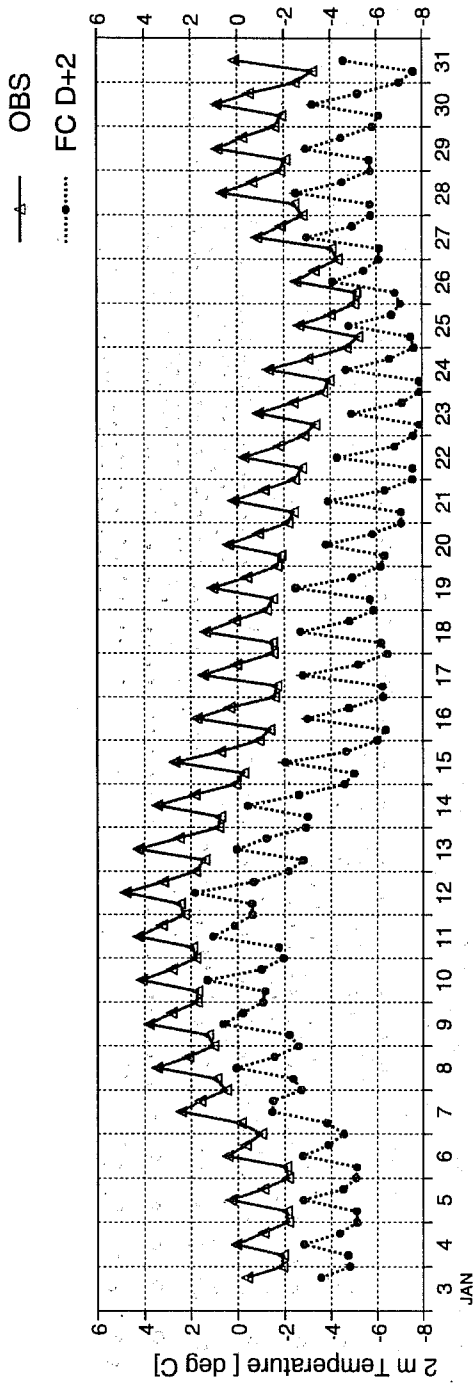

Fig. 19 As in fig. 18 but for the 2m temperature.

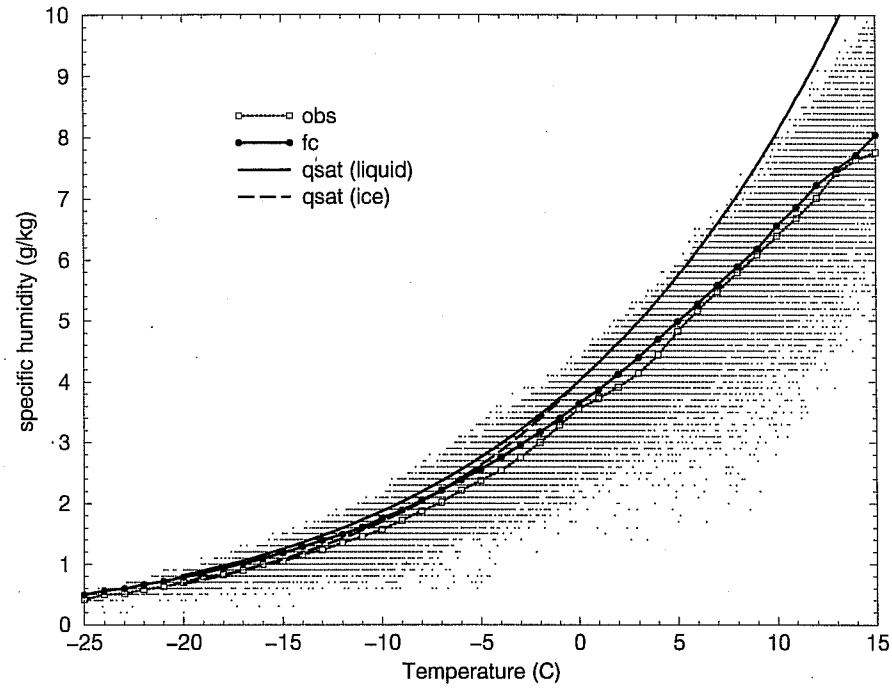

Fig. 20 The average 2 m specific humidity versus the 2m temperature (for intervals of 1°C) for the model and observations and the saturation specific humidity (for liquid and ice water) for the standard atmospheric pressure of 101325 Pa. Each dot corresponds to one model forecast.

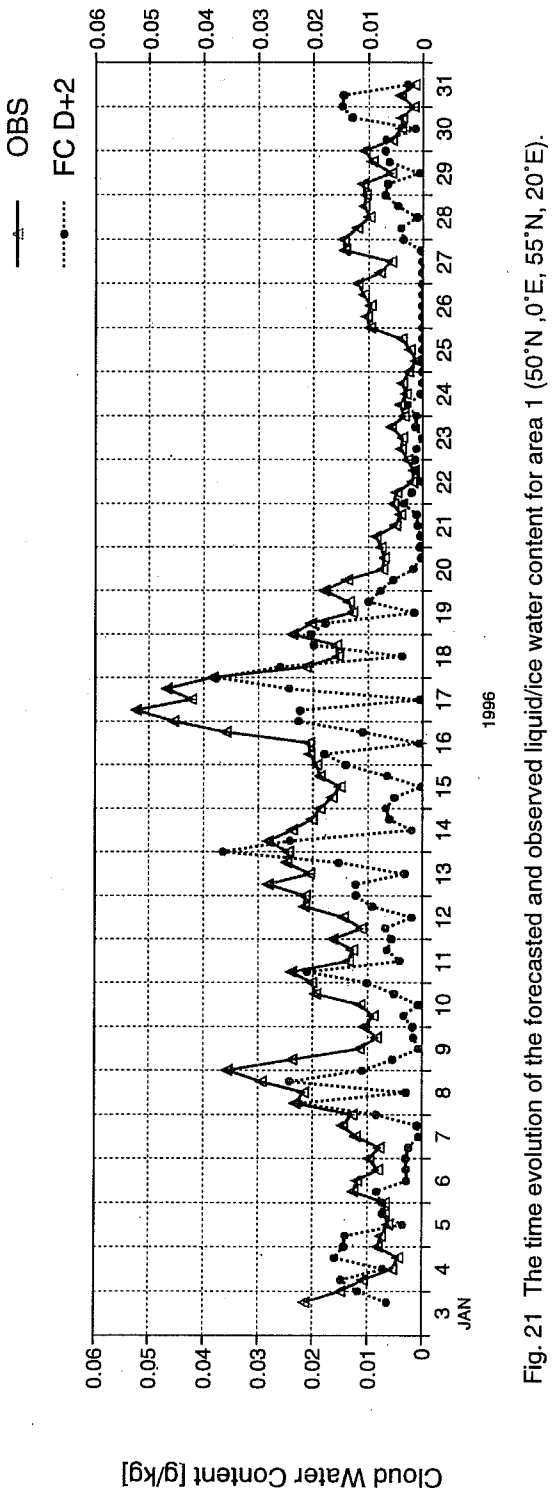

Fig. 21 The time evolution of the forecasted and observed liquid/ice water content for area 1 (50°N ,0°E, 55°N, 20°E).

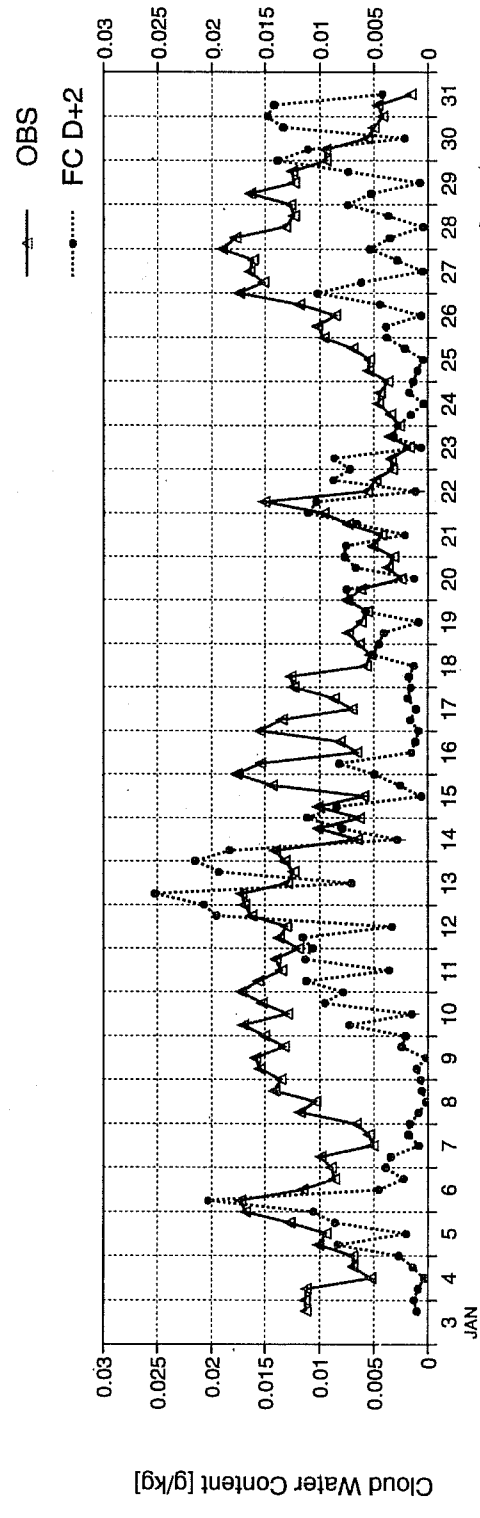

Fig. 22 As in fig. 21 but for area 2 (45°N, 15°E, 55°N, 35°E).

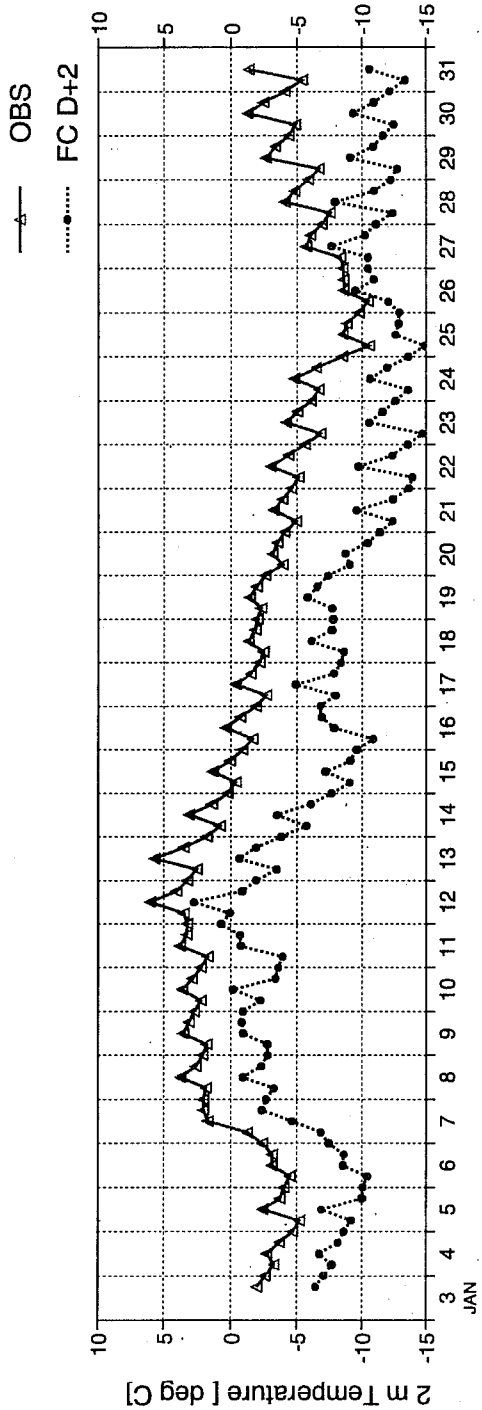

Fig. 23 As in fig. 21 but for the 2m temperature.

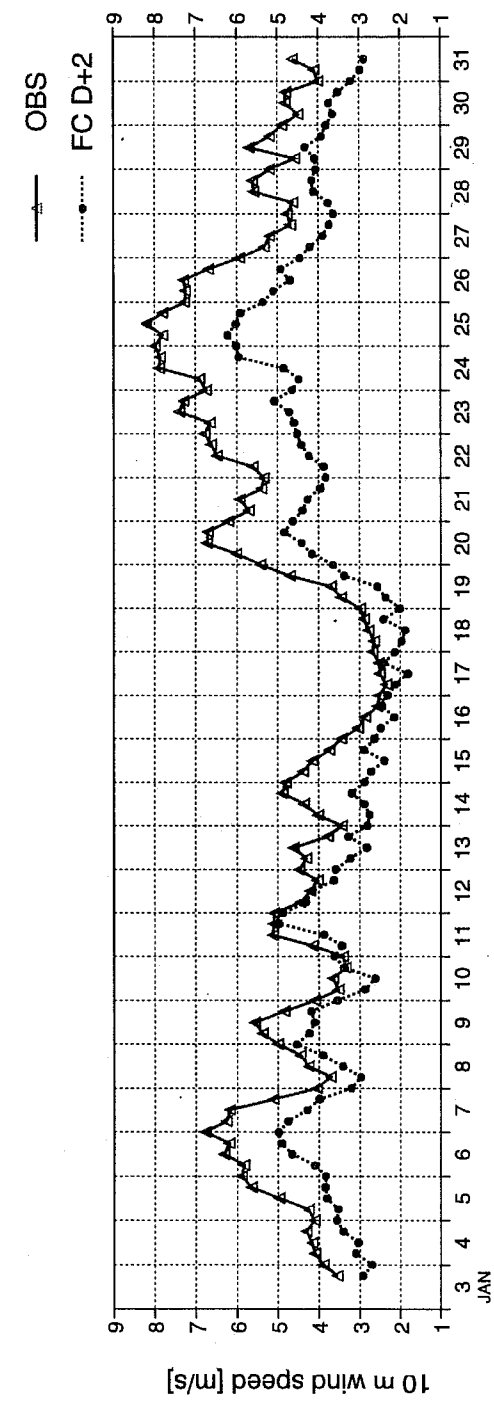

Fig. 24 As in fig. 21 but for the 10m wind speed.

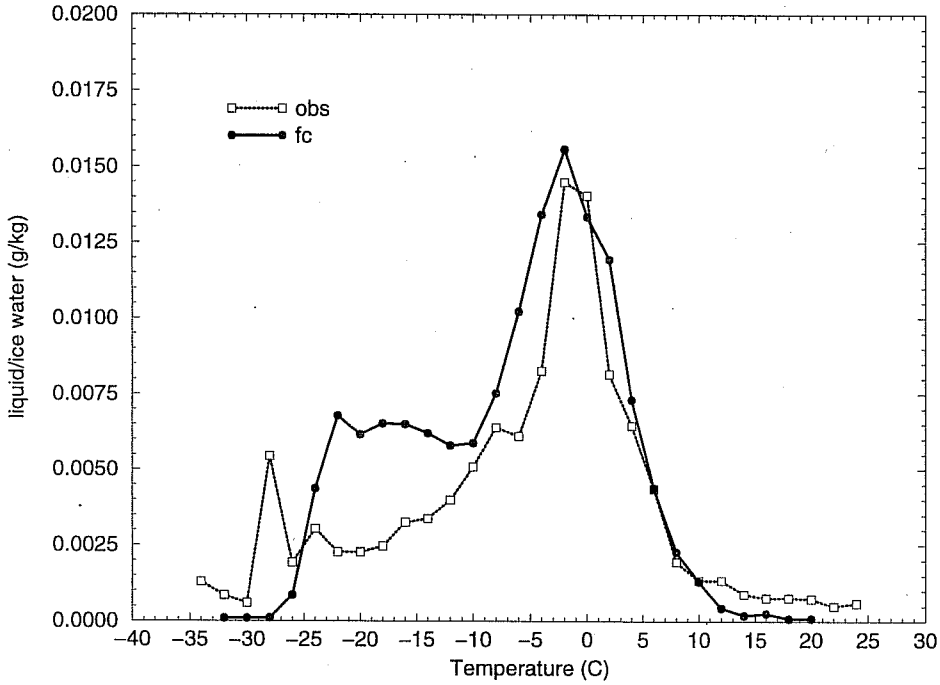

Fig. 25 The average liquid/ice water content versus the 2m temperature for the model and the observations. The average is performed dividing the temperature in intervals of 2°C and uses all the observations over Europe for the period of January 1996, which is around 100000 observations.

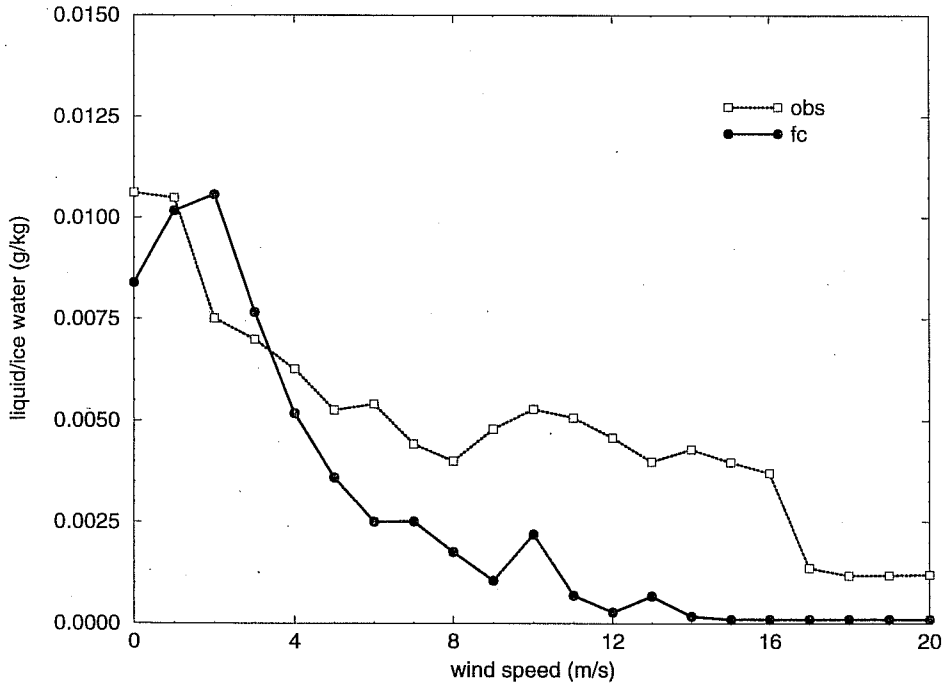

Fig. 26 The average liquid/ice water content versus the wind speed at 10 m (forecasts and observations). The average is performed dividing the wind speed in intervals of 1 m/s and uses the observations as in fig. 25.